General Response to all Referee Comments

Many thanks to the referees for detailed and constructive reviews of the manuscript. The comments have greatly helped us to improve our submission.

The referees raised following major issues:
1) lack of a clear introduction on the hypothesis/novelty/significance of this study
2) the misconceptions caused by using multiple definitions inconsistently on Light Use Efficiency (LUE)
3) unclear explanation on relative SIF
4) unnecessary and erroneous elements in the plots
5) some figures were not properly referenced in the text.

We have addressed all of the issues in the responses to individual referees and in the revised manuscript.

In general,

1) We have clarified that the central goal of our study is to mechanistically explain where, when, and why certain wavelength regions are sensitive to the canopy LUE, instead of only comparing the performance of any of our methods to the existing vegetation indices (VIs). To achieve this goal, we hypothesized that measuring hyperspectral reflectance at the canopy level can track the LUE at a sub-alpine evergreen forest. Uniqueness of our study lies in the integration of empirical analyses and process-based simulations using simultaneously measured reflectance, Solar-Induced Fluorescence (SIF), and pigment contents at the canopy level.

2) We now use GPP_{max} as the only proxy for LUE in the main text, where the other proxies of LUE at a low light intensity and daily average have been condensed and referred to the supplementary material. The relevant data and plots have also been moved to the supplementary material.

3) We rewrote the introduction to SIF and relative SIF to explain the significance and meaning of relative SIF.

4) We corrected all captions and legends in figures. The redundant legends were removed as well.

5) We reorganized the text to include necessary references to figures. The necessary analyses in the responses to referees have been added to the supplementary material.

The detailed point-to-point responses for the referee's comments are given below and reflected in the change-tracked manuscript.

Detailed response to referee #1's comments and suggestions

General comments: The manuscript "Decomposing reflectance spectra to track gross primary production in a subalpine evergreen forest" aims to investigate the link between seasonal changes in the canopy reflectance (400-900 nm) of a boreal forest and the GPP changes, measured from flux tower measurements. To do so, the authors apply a technique for decomposing the reflectance into independent components (ICA) and derive a PLSR-based factor for explaining the link with the parameter "LUEs/GPPmax".

We thank you for reviewing our work. Please find a point-by-point response below. All the changes have been reflected in the revised draft. The line numbers mentioned correspond to the revised manuscript with tracked changes.

Although the manuscript contains several interesting elements, a clear hypothesis is missing (including novel research questions) and several definitions and underlying mechanisms should be better explained.

Thank you for pointing out the lack of clarity in our hypothesis. We have made sure to clarify our hypothesis in the revised draft. The changes have been made accordingly in the abstract and introduction. In summary, we hypothesized that measuring hyperspectral reflectance at the canopy level is able to track the Light Use Efficiency (LUE) at a sub-alpine evergreen forest. For this, we used reflectance as a proxy for the contents of photosynthetic/photoprotective pigments, which was then linked to the photosynthetic LUE.

The first novelty in our study is that we continuously measured hyperspectral reflectance at the canopy level (L68-69). In previous studies, canopy level reflectance was either only simulated with radiative models or observed sparsely and mostly performed at discrete broad spectral bands. Coincident with our year-long reflectance measurements, pigments were sampled across the canopy so that we could track the onset and cessation of photosynthesis and seek to provide a direct link between changes in canopy reflectance and pigment contents at the canopy scale.

The second novelty is a comprehensive scheme to link the seasonality of photosynthesis at the canopy scale to photoprotective pigments (L66-67). This exploratory scheme includes empirical methods as well as process-based analysis. Previous studies have used

one of the two methods. However, the availability of reflectance observation, pigment samples, and flux measurements allowed us to test our hypothesis both empirically and physically.

Additionally, the PhotoSpec system we used also measures Solar-Induced-Fluorescence (SIF), which was shown to track the seasonality of photosynthetic LUE from previous studies. Thus, we included the SIF analysis to our work in order to highlight the different de-excitation pathways of excited chlorophylls by photoprotective pigments and SIF (L87-90).

For example, the authors are interested in the red-edge region where the chlorophylls absorb but don't present a clear strategy for detecting chlorophyll pigment changes (although they are later retrieved by inversion).

Thank you for asking this question. We have added the measurement of chlorophyll content in section 2.4 (L183). We measured the chlorophyll content along with xanthophyll content and carotenoid content. The chlorophyll content was used in the calculation of the car/chl ratio and the comparison against the PROSAIL inversion results. In fact, there are some changes around the red edge but the absence of clear changes in the peak Chl absorption regions points to small Chl changes throughout the season. However, these changes around the red edge could be related to Chl-a and Chl-b or structural changes. This is still an open question.

It is well known that the Car/Chl ratio is the main driver of photosynthetic behavior on a seasonal scale (L59-61), i.e. altering the ratio between energy dissipation and energy harvesting. Hence, on a seasonal scale the spectral variability would be expected to occur in the pigment absorption regions of those pigments. The authors should highlight which information can be potentially provided by their technique and how it improves (?) the tracking of GPP compared to the standardly used methods (e.g. VIs).

Our empirical methods showed and agreed on the spectral features in the reflectance were attributed to the pigments which are responsible for the photosynthetic seasonality, which was further validated by the process-based analysis using PROSAIL inversion. We have further highlighted the link among car/chl, spectral features in the reflectance, and LUE in section 3.3 (L326-331).

Although we showed the performance of our empirical methods and well-established Vegetation Indices (VIs), our goal was not to achieve a higher correlation coefficient from our method than the VIs. We have rephrased the misleading sentences (L10, L69-72), Instead, our work focuses on mechanistically explaining where, when, and why certain wavelength regions are sensitive to the canopy LUE, which validated the high/low correlation coefficients from the VIs (L63-66).

Further, the authors aim to evaluate the pigment driven spectral changes (where, when

and why). In this regard the authors could further highlight the seasonal dynamics of the detected components in respect to the spring recovery in boreal forests. Does it provide more info compared to the VI dynamics?

> Thanks again for pointing out our unclear discussion on comparing our methods with VIs. We strengthened our discussion in the revision (L46-53, L353-356). In section 3.5 comparison across methods, what we really wanted to highlight is the difference between the reflectance change driven by the pigments and SIF. Since the spectral shape and CCI (the representatives of other VIs) both related to the chl:car ratio, the same behavior from the spectral change and CCI are, in fact, expected in Figure 9. Interestingly, the PLSR and ICA decompositions didn't significantly improve (or provide more info) to the ability of existing VIs. This is important because it validates the idea that 'simpler' approaches might be sufficient for tracking the seasonality in evergreen systems.

Finally, there are several jumps in the storyline, use of unclear terminology/method descriptions (L141-143, L190-194) and missing parameters definitions (L187). The presentation of the results is sometimes fragmented (L183-185) or not clear from the graphs (L217-L218, GPPmax is not shown). All these aspects need to be thoroughly reviewed before acceptance of the manuscript.

> Thank you for the comment. In the revision, we have corrected the definitions, kept the consistency of terminology, and made sure the plots are explanatory to the text. Please see the change tracked revision for details. Some of the changes are made in L163-166, L226-229, L216-219, L209-L212, and L243-253 with respect to the examples that the referee mentioned.

Specific comments From L43-48 it could be misunderstood that LUE of deciduous forests is not affected by biotic factors, while LUE changes due to e.g. pigment composition occur in combination with structural changes, which in fact you can also term a "biotic" factor. The term "biotic" refers to higher-level ecosystem interactions and is less appropriate in the LUE-photosynthesis terminology here. Please rephrase.

> Thanks for this comment. We have referred to changes in pigment compositions as 'needle biochemistry' (L47).

What is the link with the "differentiation in NPQ pathways" and SIF, which are suddenly mentioned at L75. Is this relevant for seasonal patterns/this manuscript?

> We have rewritten this section in the revised manuscript and explained the necessity of the comparison of SIF and reflectance spectra (L46-53, L82-90), where the definition of NPQ has been carefully rephrased. SIF has been shown to track the photosynthetic seasonality in previous studies. However, SIF and the spectral change in reflectance represent different de-excitation pathways of excited chlorophyll. PhotoSpec measures

both hyperspectral reflectance and SIF, which enables us to compare the seasonality captured by these pathways.

L77: you are comparing fluorescence radiance with reflectance, which varies strongly in the 400-900 region and is moreover a ratio, not a radiance to compare SIF with.

In the analysis, we used relative SIF, which is SIF normalized by the reflected near-infrared radiation. In the revision, we have rephrased the paragraph and introduced the relative SIF in this section (L82-90). Relative SIF is used to account for sunlit/shaded fraction within our observation FOV, since it provides an indicator of how 'bright' the area of interest is.

L215-216: why would low PAR not drive photosynthesis? Please reformulate this sentence, pointing to the controlling factors in winter/spring.

Thanks. The original sentence was trying to inform the readers that GPP was near zero in winter, although the PAR level in winter is not. This matches with the strong seasonality of our LUE measurement, GPP_{max}. And figure S3 shows that instead of PAR, T_{air} is one of the controlling factors in winter. We have rephrased it in the revision (L239-242) to make it clearer.

L78-81: The mechanisms are not clearly explained here. What about the seasonal radiance budget, i.e. the "abiotic" factors?

Thank you for pointing out the missing part of SIF. In the revised draft, we have elaborated on the explanation of SIF mechanisms and introduced relative SIF (L52-53, 82-90). While there is still enough light to drive photochemistry in winter, frozen boles limit water transport as needles must dissipate excess energy as heat. The primary mechanism for increased NPQ is through sustained energy dissipation by photoprotective pigments which co-varies seasonally with SIF (Magney et al., 2019).

Methodology After filtering the data based on light conditions and snow, how many winter days actually remain? Please mention the amount of samples, for both winter and growing season, also in Fig. 1.

We have 96 days of spectral samples between DOY 100-300 and 115 days of spectral samples in the rest of 165 "winter" days.

In the pigment analysis, we have 6 days of both spectral and pigment samples between DOY 100-300 and 4 days in the rest of 165 "winter" days.

In figure 1, there are 39 days in the growing season and 113 days in the dormancy.

These statistics have been included in the revision (L132 and Fig. 1).

Relative SIF: please elaborate on how the normalization is done (raw data, wavelength range). Since you argued in the introduction that the structural changes are less an issue for coniferous forest, what is the true (or expected) impact of this normalization for SIF? What is the difference with not normalizing? Did you quantify this?

We have added the description of relative SIF in L152-155. Relative SIF is SIF normalized by the reflected near-infrared radiance at 755 nm. This normalization will make SIF more comparable to a 'SIF yield', as it is a ratio effectively correcting for incoming irradiance, and sunlit/shaded fraction (see above). It also eliminates most of the directional effects within the canopy. The attached plot (added to supplementary material) is similar as we did in Figure 5d but with SIF and relative SIF. The seasonal cycles of relative SIF and SIF are well correlated. Relative SIF is more correlated with the GPP_{max} in seasonal variations. However, the sub-seasonal change in the growing season is captured more by relative SIF.

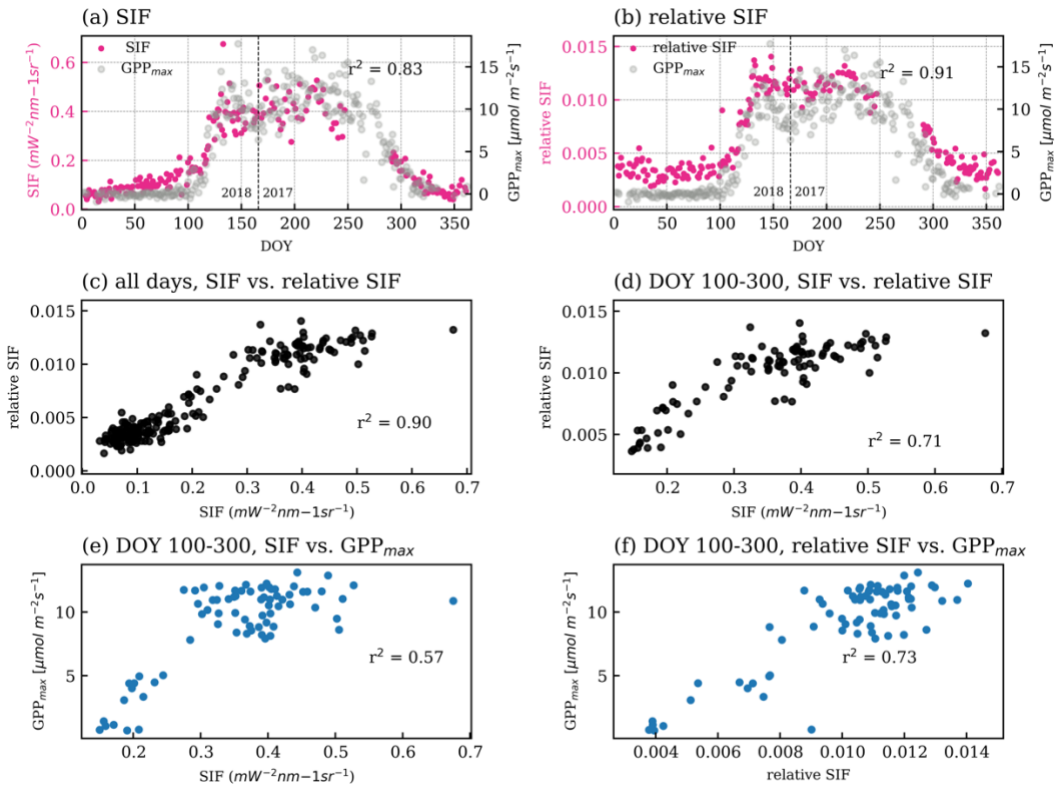

LUElightL/LUEtotal: these are supposingly daily values? How APAR was defined/calculated based on the raw data and show a plot of the methodology described in L160. Moreover these parameters are not clearly presented later on and Fig.2 does

not give a sufficient visual on the calculation/importance of these parameters. Are they relevant for the story?

GPP_{max}, LUE_{lightL}, and LUE_{total} are light use efficiencies (LUE) at different abiotic status: 1) GPP_{max}: light-saturated LUE; 2) LUE_{lightL}: light-limited LUE; 3) LUE_{total}: mean status LUE. They are all calculated as daily values. To make the discussion concise and clear in the revised draft, we only showed the results of GPP_{max} to represent LUE in the main text as it is more representative than LUE_{lightL} and more physiology-driven than LUE_{total}. We have made sure the terminology of using LUE and GPP_{max} is consistent throughout the draft. We also added sections on how APAR, LUE_{lightL}, and LUE_{total} were calculated in the appendix with visualized explanations.

APAR was calculated from seven pairs of PAR sensors installed. One pair of sensors was installed above the canopy on the same tower where PhotoSpec is located (measuring incoming PAR and reflected PAR). The other six pairs of sensors were installed below the canopy (measuring reflected and transmitted par). The derivation of APAR is shown in the following graph.

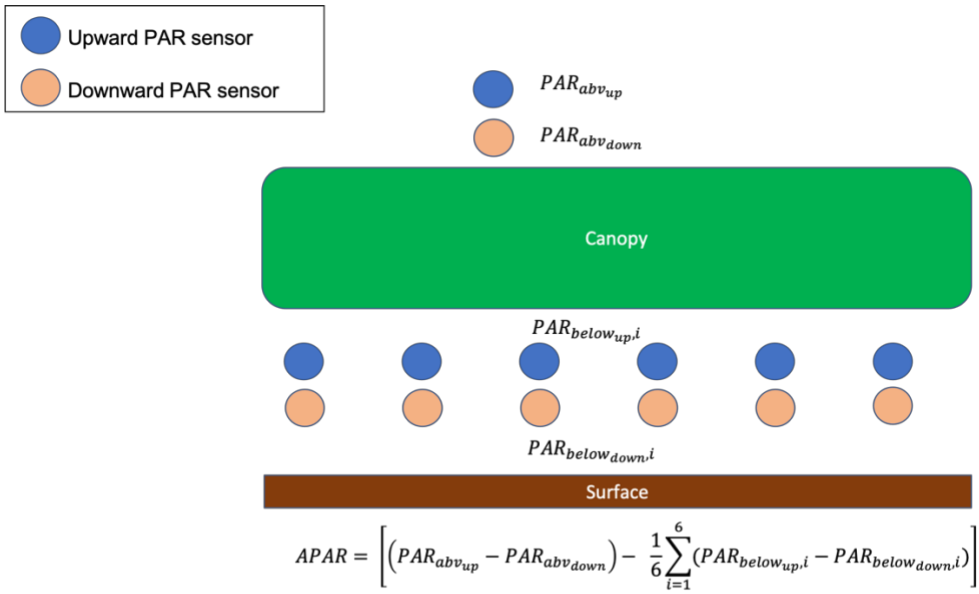

Here is a demonstration of how LUE_{lightL} and LUE_{total} were calculated. Given a day (DOY =278 as an example), we selected the GPP measurements when the PAR level is between 100-500 µmol m-2 s-1. Then, we did a linear regression of those GPP measurements with their APAR levels (the cyan dots and dashed line). The slope of this regression is LUE_{lightL}. On the same day, all the GPP measurements that happened when the PAR level is above 100 µmol m-2 s-1 are the orange crosses in the plot. We calculate the ratio of GPP and APAR of those orange points, and the daily mean of the ratio is the LUE_{total}.

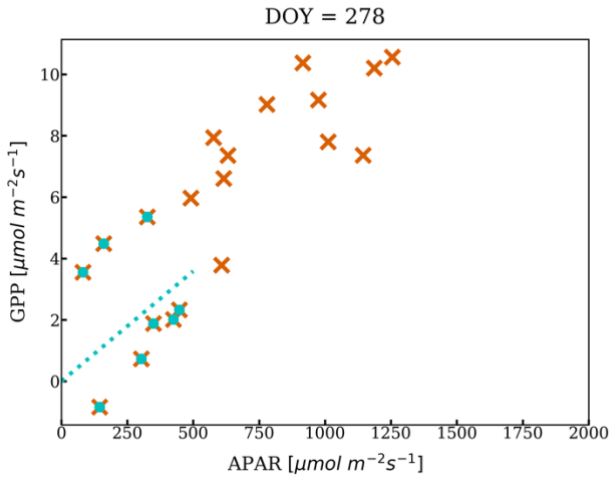

L155: It is claimed that PAR levels between 1000 and 1500 µmol m-2 s-1 are reached throughout the whole year, but that is not what is seen from Fig. 3, showing PAR values hardly exceeding 1000 mol m-2 s-1. LUEs: this parameter suddenly appears at L187, without any previous definition! Also, what does the reader need to understand from the LUEs/GPPmax parameter? Please, elaborate the choice of this parameter and how it should be interpreted in terms of vegetation dynamics.

In Fig.3, PAR is low because it was calculated as the daily averaged PAR of above 100 µmol m^{-2} s^{-1}. In the calculations of GPP_{max}, LUE_{lightL}, and LUE_{total}, PAR and APAR are half-hourly data.

Thank you for catching this error. LUEs referred to LUE_{lightL} and LUE_{total} in the discussion paper. And LUEs/GPP_{max} refers to GPP and LUEs. GPP_{max}, LUE_{lightL}, and LUE_{total} are light use efficiencies (LUE) at different light regimes: 1) GPP_{max}: light-saturated LUE; 2) LUE_{lightL}: light-limited LUE; 3) LUE_{total}: mean status LUE. We did all the analysis with these three parameters. The results were quite similar in terms of the seasonal cycle. As we explained in section 3.1 (L168-171 and section 2 in the supplementary material), GPP_{max} is a better proxy for LUE as it is more representative than LUE_{lightL} and physiology-driven than LUE_{total}. Thus, we decided to only keep GPP_{max} in the main text. In the revision, we made sure to use GPP_{max} consistently.

Pigment contents: is there a reason why Chlorophyll content is lacking? This does not follow the line of the objectives.

We didn't show chlorophyll content in figure 7 because Bowling et al (2018) and Magney et al (2019) have shown chlorophyll content didn't vary with the season in our study site. However, we agree with your suggestion that it is important to include it to comprehensively discuss the importance of car and chl:car ratio to the seasonality of

photosynthesis. We have discussed the measurement of chl (L183, L216-218, L339-341) in the revision.

L190: rephrase this sentence for a better understanding of the final aim. The resulting coefficient is given somewhere or expected later in the results? Which four PLSR components are you referring to?

Four PLSR components we mentioned are the parameters used when we trained the PLSR algorithms. We have rephrased the paragraph to explicitly describe the PLSR coefficient and its role in our analysis with mathematical expressions and clarified terminology (L204-221).

L203: the raw input reflectance data is unclear here. Also, please further highlight which pigments you are inverting from the reflectance and why.

Thank you for comments. When we calculated the Jacobians, we used the log-scaled daily-averaged reflectance from PhotoSpec. In PROSAIL inversion, we used the daily-averaged reflectance without log scaling. The inverted pigments are chlorophylls, carotenoids, and anthocyanin. We compared the inverted pigment contents of chlorophyll and carotenoids as well as their ratio to the measurements from needle samples. We clarified this in the revised draft (L230-231) and provided all averaged reflectance data as supporting online material.

Results Section 3.1: this whole section refers to results about GPP max without clearly referring to results on this parameter. Please refer better to the results shown in Fig. 3 and check why LUElighL and LUEtotal are not shown in the graph (but mentioned in the legend).

L226: please refer first to the observations in the figure in the main text, and for further details refer in addition to the supplementary figures.

Thank you for catching the misleading legend (Fig. 3). We have removed it and referred to the plots in the supplementary in the revision.

Fig. 4: “Annual mean reflectance”: correct this as the “Annual mean log scaled R”

Thanks. We have corrected it in the revision (Fig. 4).

Section 3.2: The link between the seasonality of the spectral components and GPP max seems interesting, but there is a clear difference in the onset of the components 1 and 2 (the more dynamic ones) which might be in addition highlighted and of scientific interest.

Thank you for catching this. We are not sure the origin of the abrupt onset near DOY 50 in component 1. This abrupt change happens in all three components in Fig. 4. We suspect the change was caused by background noise, such as snow from the ground, given that the PhotoSpec system operated normally during that period. However, we cannot identify the reason and suggested this as mere speculation in the revisions (L297-300).

Section 3.3: The explanation of the methodology in this section needs to be improved.

We have elaborated the implementation of PLSR analysis in the revision (L204-L218).

Please be more concrete in terminology (L278: transition period, noise) and what exactly you are referring to.

The transition period refers to the onset and cessation of growing season shown in GPP_{max}. The noise refers day-to-day fluctuations in winter. GPP_{max} was consistently near 0±1 µmol m^{-2} s^{-1} before DOY 100, while PLSR reconstructed GPP_{max} varies from -2 to 5 µmol m^{-2} s^{-1} in the same period. This large variation is from the noisy input of reflectance, which can be seen in the ICA components. We rephrased the sentence to be more specific (L305-309).

L279-L281: What do you mean with that the high-frequency variations are not captured by any method? The PRI captures the variation of the most dominant feature in the PLSR coefficients. So why would these variations not be related to pigment content?

The high-frequency variations refer to the day-to-day fluctuations within growing season. Both PRI and PLSR coefficients are relatively flat during the growing season. They did not follow the day-to-day variations within the season. As both PRI and PLSR use the pigment absorption feature, their invariance suggests these variations are less relevant to pigment. The specific changes have been made in L305-309.

Section 3.4: L302: Please refer to the graphs.

Thank you for the comment. The sentence has referred to Figure 8(c) (L338-339).

Detailed response to referee #2's comments and suggestions

This paper presents an exploratory study of a very nice data set studying 400-900 nm reflectance, fluorescence, and GPP along with other ancillary measurements including carotenoid composition at leaf scale at the Niwot Ridge, Colorado, USA site in a sub-alpine evergreen forest. As I don't believe this complement of data has been presented

at such a site, the data analysis is appropriate for publication in Biogeoscience. However, there are several details that must be addressed before the paper is acceptable for publication. As the first reviewer provided a number of suggestions, this reviewer will try to present a few points not already covered there. The paper contained many small errors that, while minor, led to making the paper a difficult read. Hopefully this will be fixed in a revision. Otherwise I found the paper to be very informative and interesting.

Thank you very much for your generous comments. We appreciate you recognized the novelties in our work. We apologize for all the confusion from mislabeled plots and complex phrases. We have included a point-by-point response. The line numbers mentioned correspond to the revised manuscript with tracked changes. The corrected plots, as well as responses, have been incorporated in the updated version of our manuscript.

General comments: I have two main issues with the paper. The first is that SIF contains a component of PAR while reflectance does not. This makes it a bit unfair to compare any of the reflectance- based quantities directly with GPPmax (similarly affected by PAR as is SIF) and also to derive the PLSR reconstruction of GPPmax without consideration of PAR. It may be fine to do the reconstruction of other quantities (related to pigments) without account of PAR, but generally not GPPmax. A much better result may come from normalizing GPPmax with respect to PAR (or daily averaged PAR or daily averaged potential PAR) and performing the reconstruction on this quantity. This is particularly important in Fig. 9. Some statements may need to be modified after taking into account PAR (e.g., paragraph starting on L. 320).

We apologize that we did not properly introduce the relative SIF in the introduction. In figure 5(d) and figure 9, we accounted for PAR impact on SIF by using relative SIF, which is SIF normalized by the reflected near-infrared. We have rewritten the introduction as well as methods on relative SIF to clarify this (L52-53, L82-90, 152-155).

We agree with you that normalization is necessary. We used Eq. (1) to derive light use efficiency (LUE), which is inevitably conditioned on PAR and fPAR. Benefiting from the APAR measurements we have, we can use in situ APAR as the normalization factor instead of PAR and presumed fPAR in previous studies. According to the light response curve of photosynthesis (figure 2), we summarized three different scenarios LUE: 1) light-limited (low light, LUE_{lightL}); 2) carboxylation rate-limited (high light, GPP_{max}); and 3) daily average (LUE_{total}).

LUE_{lightL} is the fitted slope of GPP and APAR when PAR is between 100-500 µmol m^{-2} s^{-1}. The fit was forced to go through the origin as the equation has no intercept.

LUE_{total} is the daily average of GPP/APAR during the day.

Theoretically, we could calculate GPP_{max} similar to what we did for LUE_{lightL}, i.e. regressing GPP against APAR when PAR is saturated. Unfortunately, there is a 26-day gap in APAR measurement in the beginning period of our study. We could also normalize GPP by PAR, as you suggested. Yet, it requires assumptions about fPAR, which brings uncertainties.

Considering GPP often flats out when PAR is greater than 1000 µmol m^{-2} s^{-1}, the slope of fits could be biased by the spread of data point. Thus, we defined GPP_{max}, the average GPP within a moderately narrow window of PAR (1000-1500 µmol m^{-2} s^{-1}), to represent the LUE when the carboxylation rate is limited. In this way, we achieved normalizing GPP without missing more data because of APAR.

Those two different definitions of GPP_{max} are significantly linearly correlated (in fig.AC2.1 in this response document). If GPP_{max} is defined as the average of normalized GPP by PAR (y-axis), the analyses on the seasonal cycle will differ little from GPP_{max} defined as mean GPP at high PAR (x-axis). Although GPP normalized by PAR results in the correct unit of LUE, it is easily mistaken as fPAR has been considered. To avoid this confusion, we chose to use mean GPP at PAR between 1000 and 1500 µmol m^{-2} s^{-1}.

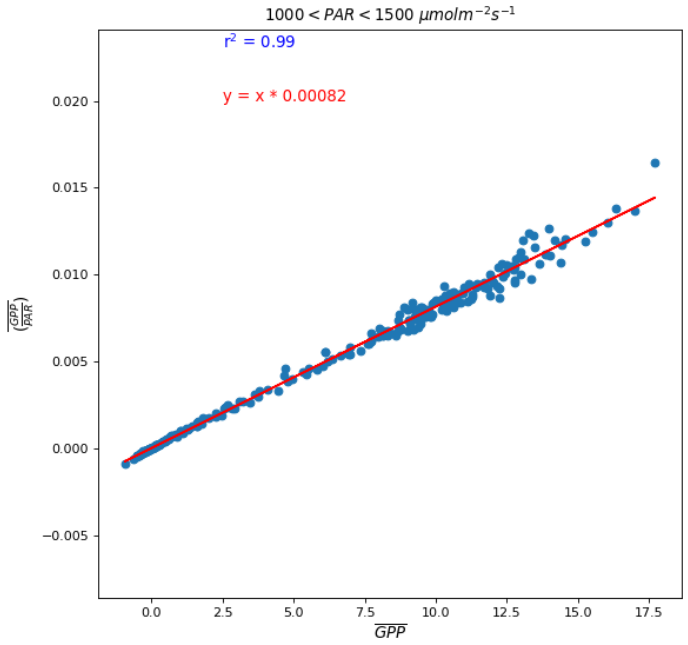

Figure.AC2.1 Two ways to calculate GPP_{max}.

We also tested the LUE defined in three scenarios: LUE_{lightL}, GPP_{max}, and LUE_{total} for all the analyses in the manuscript. They behave similarly. We considered that needles spent more time at highlight intensity in the daytime. Hence, we decided to use GPP_{max} as the only proxy of LUE in the main text. We kept the other two matrices to the supplementary. The labels were misleading in the main text. We have cleaned them up in the updated draft (Fig. 3).

The second comment relates to the terminology around the component analysis. It would be helpful if the reflectance can be written in the form of equations explaining the decomposition. Then it may be more clear to express what is being plotted. In my understanding of the terminology, a coefficient should be a number multiplied by a particular spectral component to reconstruct a given spectrum. The term temporal component is confusing to me as this is not what has been decomposed, but rather it is the coefficient of a given spectral component to reconstruct a spectrum observed at a particular time if I have understood correctly. The labeling of Fig. 6 is particularly difficult to understand since panel (a) shows much more than PLSR coefficients. The line labeled GPP_max would be more clear if it had PLSR coefficient in the label.

Thank you for the advice. We have changed "temporal components" to "temporal loading" (Eq. (4) and L201). We added the following expressions to the draft:

ICA:

$$-log(R_{\lambda,\mathrm{DOY}}) = \sum_{i=1,2,3} (\text{spectral component}^{\,i}_{\lambda} \cdot \text{temporal loading}^{\,i}_{\mathrm{DOY}}).$$

PLSR:

$$\mathrm{GPP}_{\mathrm{max,DOY}} = -log(R_{\lambda,\mathrm{DOY}}) \times \text{PLSR coefficient}^{\mathrm{GPP_{max}}}_{\lambda}.$$

Specific comments:

L. 118. VI's are normalized such that at least some of the solar geometry effects are removed. This may not be the case for reflectance in general.

Thank you for pointing this out. We agree the experiment related to this sentence is not enough to clarify the BRDF impact on reflectance. Thus, we did a PLSR analysis on individual measurements of phase angle and reflectance for 3 summer days (2017-7-1 to 2017-7-3), such as fig.AC2.2.

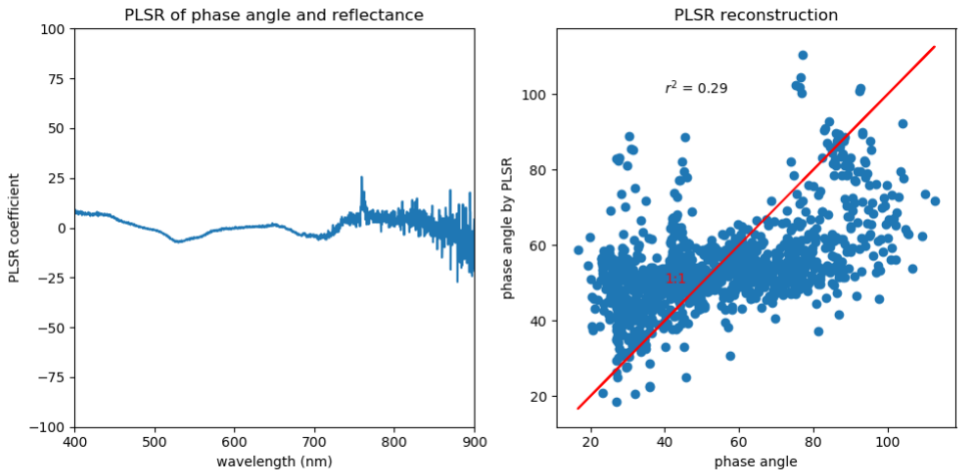

Figure.AC2.2 PLSR analysis on phase angle and reflectance.

Indeed, the reflectance has different sensitivities to the phase angle. However, the poor correlation of PLSR reconstructed phase angle and the measurement one suggests the variations in phase angle should not be the critical factor for the change in reflectance. In our manuscript, we primarily removed the bi-directional impact by averaging all the individual reflectance that was measured at different solar geometry and viewing geometry. This analysis has been referred in L128-129 in the revision.

L. 142. Normalized at which wavelength(s) exactly? I'm not sure I agree that normalizing by reflected radiation is going to properly "account for the complexity of signal due to canopy structure" at this particular site. Please provide more justification of this statement.

Thanks for pointing out this misleading sentence. SIF was normalized by reflected near-infrared radiation (755 nm) to account for the sunlit/shaded fraction within our observation FOV. Benefiting from the small FOV of PhotoSpec, we think the complexity of canopy structure has minimal impact on our signal. We have clarified the statement in L85-90.

Since it is mentioned on L. 183 that 3 components explain more than 99.99% of variance, can you state how much variance is explained by each of the components shown.

Because ICA minimizes the dependencies of the second-order moment (variance) and higher, the randomness during the minimization makes the explained variance and order of individual component unclear. In our calculation, the ICA algorithm reduced the dimension of the input matrix by eigenvalue decomposition first, from which the first three second-order independent/orthogonal components yielded 99.99% of the variance. Then, the algorithm extracted the independent components of high-order moments from

these orthogonal components. We have included this explanation in section 4 in the supplementary material.

L. 261, it is mentioned that T_{air} and VPD covary with GPP_{max}. Please provide some numbers here such as correlations.

We have cross referenced the figures in the supplementary in the draft (L246, L252) while we also included the following the Pearson-r2 value of correlations.

During the growing season:

GPP_{max} and VPD = 0.34

GPP_{max} and T_{air} = 0.24

PRI and VPD = 0.04

PRI and T_{air} = 0.02

I am confused as to what is meant by "short-term" on line 262 as a few lines above it is said to be the smoothest. Some may take short-term to mean daily. In that case, we wouldn't expect it to be smooth.

Thanks for the feedback. We meant to use "short-term" and smoothness to refer day to day or sub-seasonal variations. We have revised the paragraph with a consistent description in the updated manuscript (L305-309).

Have you definitively shown here that the green band captures variations in LUE? Isn't this only inferred?

Yes, we inferred the green band capturing LUE by the good performance of GCC. We changed the word "show" to "suggest" (L294).

Fig. 5, something appears incorrect with the r2 value shown in panel (f).

We found a bug in the calculation and corrected it (Fig. 5). The correct r2 values of GPP_{max} with CCI, PRI, GCC, relative SIF, NDVI, and NIRv are 0.85, 0.81, 0.73, 0.87, 0.06, and 0.40, respectively.

L. 319, What exactly is meant by diurnal? The most common use of this word in my

field pertains to “of or during the day” which is commonly taken to mean sub-daily.

Yes, it means day-to-day/sub-daily variations here, similar to the previous comment. we have made sure the wording is accurate and consistent (L353-357).

Same paragraph: In this work, it is not definitively shown that SIF tracks seasonal or diurnal variations better than reflectance. While SIF shows slightly higher r2, the differences were not shown to be statistically significant. It is curious that CCI gives a higher r2 value with respect to GPPmax than the PLSR analysis and the PRI gives the same value as PLSR. Also the sample of points looks different in Figs. 5 and 6.

Thanks for the suggestion. The phrase appears to make readers think we are competing with existing methods, which is misleading. Our study focuses on mechanistically explaining where, when, and why certain wavelength regions are sensitive to canopy LUE seasonality. Thus, a similar performance from CCI and PLSR is expected as CCI uses the most sensitivity band. Although SIF represents a different process from the reflectance-based methods the good performance of relative SIF has been discussed in Magney et al., 2019, which makes Niwot Ridge a very interesting site to study.

After we corrected the calculation, relative SIF and PLSR (r2= 0.87) have the highest r2 compared to other indices, although not significantly. CCI and PRI are comparable but less correlated with respect to GPP_{max} than PLSR. The different reference bands used by CCI and PRI might cause the slight difference in their correlation with PLSR.

The difference in Figs. 5 and 6 were because We only plotted the observed GPP_{max} when the reflectance is also available in Fig 6, while all the observed GPP_{max} was plotted in Fig 5. In the revised draft, these two plots are consistent as Fig 5.

Fig. 9: There is no goodness of fit metric here relative to measurement uncertainties. To make it more clear the fits should be shown with the observations and the residuals and fit properly evaluated with standard metrics. Otherwise the differences are not convincing.

Thank you for the suggestion. We attached a plot of individual fittings and their evaluations (fig.AC2.3, Fig.D1). The fitted curve has been expressed as the derivation in Appendix D. The pearson-r_2 and p values listed in each subplot were calculated from the correlation of observed and fitted variables. The residual was calculated as the average L2 norm of the difference between observed and fitted variables normalized by the observation. The fittings are overall good. Because the ICA component lacks a clear sigmoid shape, ICA has a larger residual.

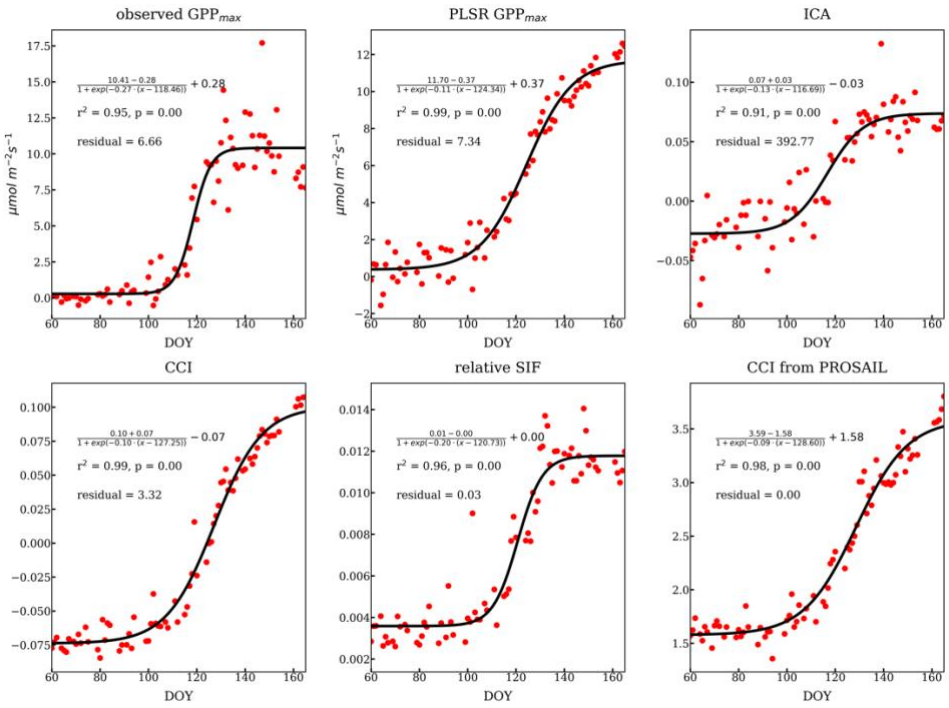

Figure.AC2.3. Individual sigmoid fits of timeseries of interest. The fitted curves are expressed in the format as appendix D. The pearson-r2 and p values are for the observed and fitted variables. The residual is

$$\frac{1}{n}\sum_{i}(\frac{x-\hat{x}}{x})^2,$$

where x is the observed value and $\hat{x}$ is the fitted value.

L. 334, I may have missed something but I didn't see how this feature was shown to be directly related to LUE in the paper. This may be inferred but it wasn't directly shown.

We are now more precise in phrasing. The sentence (L371-373) has been changed to "The main spectral feature centered around 530 nm is most important for *inferring* the seasonal cycle of reflectance (400 – 900 nm) and LUE, which corresponds to changes in carotenoid content."

Detailed comments:

There are a number of typos that need to be fixed, for example subscripts (L. 1, L. 226, L. 234, Fig. 3, Fig. 6 panel (b)).

Thanks a lot for catching them. We have corrected the typos and made sure all the subscripts are coded correctly in the revision (L1, L239, L244, Fig. 3, and Fig. 6(b)).

There are a number of statements that need to be clarified or corrected for language (see L. 2, for example, "Estimating . . . is a primary uncertainty" would be better phrased as "Estimation of...corresponds to a primary source of uncertainty" or similar). See also lines 11-12 (unclear sentence, L. 14, etc.).

We have rephrased those unclear sentences and be more precise (L2, L10-13).

Line 21: Satellites do not measure GPP, rather GPP can be inferred and usually make use of other data.

The sentence is now more precise in the updated draft (L24).

It's a little confusing in L. 159 to start with "To implement Eq. (1), then define a particular case for Eq. (1). Please rephrase.

We rephrased the sentence as "We followed the format of Eq. (1) to define light-limited LUE (LUE_{lightL}) as…" This paragraph has been presented in section 2.2 in the supplementary instead of main text.

L. 164-166. It's not clear at this point what the meteorological data are included for. L. 165 would be more clear to say that daily mean . . . were computed from . . ..

We replaced "meteorological variables" with "Air Temperature (T_{air}) and Vapor Pressure Deficit (VPD)" in L148. And, rephrase L164-166 as daily T_{air} and VPD were computed from averaging half-hourly T_{air} and VPD when…" The rephrased sentences are in L176-178 in the revised manuscript.

The first reviewer was unclear about what LUEs/GPPmax is. I think I figured it out but it took a lot of time and was very unclear.

Thanks for taking the time to sort it out. We apologize for the confusion. In the updated draft, we have clarified the usage of acronym LUE with GPP_{max} as the only proxy for LUE in the main text. The results for LUE_{lightL} and LUE_{total} are put in the supplementary.

Line 217. Is LUElight the same as LUElightL defined above?

Yes. Sorry about the typo.

L. 226: Confusion regarding Fig. 3 (not S3) but also most of which is repeated in Fig. S2 but with the lines that are referred to in Fig. 3. Suggest to include only one figure with all the lines (in the main manuscript). A similar thing happens with Fig. 9 and D1. Suggest to include only one of these.

We have only included Fig.3 and Fig.9 in the main draft and eliminated Fig.S2 and Fig.D1.

Fig. 3: Specify that these are daily-averaged quantities?

We have specified them in both the caption in Fig. 3.

Fig. 4 caption: Only the 2nd component shows the carotenoid Jacobian.

Yes, because we want to emphasize the similarity of component 1 with the chlorophyll jacobian only. We have corrected the caption in Fig.4 and made sure it is consistent with the plot.

Sect. 3.2, first par. There is a lot of information in this paragraph. It might be more effective if it was split up.

Yes, we agree with you that is too tedious to read. We have split it into paragraphs and rephrased with the equations of ICA so that it is more clear.

L. 268, the word "thus" here is confusing.

We have removed "thus" from the sentence (L293).

Fig. 6: Panel (a) labeling is very confusing. First, the title of panel (a) as well as the label on right side is confusing as these are not really coefficients are they, they are either components of combinations of components (caption is also unclear)? The caption states that the overlaid solid line is the 2nd ICA component, but there are two solid lines. The blue line in the legend is labeled as GPPmax, but it isn't really GPPmax as labeled in the bottom. Would suggest to just remove the titles of both panels.

Thank you for pointing this out. In fig. 6(a), we have changed the label of "GPP_{max}" to "PLSR coefficient". The blue curve indeed is the coefficient when the PLSR is written in a fashion of linear model, such as:

$$\mathrm{GPP}_{\mathrm{max,DOY}} = -log(R_{\lambda,\mathrm{DOY}}) \times \mathrm{PLSR\ coefficient}_{\lambda}^{\mathrm{GPP_{max}}}.$$

However, the y-axis on the right is only for PLSR coefficient not for ICA. We clarified that both Jacobians and ICA component were scaled in the caption in Fig. 6.

The solid blue line is the PLSR coefficient. The solid orange line is the 2nd ICA component. We have clarified them in the revised draft. The titles were also removed.

L. 297 should be “support”.

We have corrected it (L333).

It would be better to subscript the small letters in Cchl, Ccar, and Cant.

We have subscripted them in the revision.

Fig. B1 caption should say theoretical maximum (or clear sky)

We have changed it to “theoretical maximum” in the revision (L410 and Fig. B1).

Decomposing reflectance spectra to track gross primary production in a subalpine evergreen forest

Rui Cheng[1], Troy S. Magney[1,11], Debsunder Dutta[2,12], David R. Bowling[3], Barry A. Logan[4], Sean P. Burns[5,6], Peter D. Blanken[5], Katja Grossmann[7,8], Sophia Lopez[4], Andrew D. Richardson[9], Jochen Stutz[8,10], and Christian Frankenberg[1,2]

[1]Division of Geological and Planetary Sciences, California Institute of Technology, Pasadena, CA, USA
[2]NASA Jet Propulsion Laboratory, California Institute of Technology, Pasadena, CA, USA
[3]School of Biological Sciences, University of Utah, Salt Lake City, UT, USA
[4]Department of Biology, Bowdoin College, Brunswick, ME, USA
[5]Department of Geography, University of Colorado, Boulder, CO, USA
[6]National Center for Atmospheric Research, Boulder, CO, USA
[7]Institute of Environmental Physics, University of Heidelberg, Germany
[8]Joint Institute for Regional Earth System Science and Engineering, University of California Los Angeles, Los Angeles, CA, USA
[9]Center for Ecosystem Science and Society, and School of Informatics, Computing, and Cyber Systems, Northern Arizona University, AZ, USA
[10]Department of Atmospheric and Oceanic Sciences, University of California Los Angeles, Los Angeles, CA, USA
[11]Department of Plant Sciences, University of California, Davis, CA, USA
[12]Department of Civil Engineering, Indian Institute of Science, Bangalore, India

Correspondence: Rui Cheng (rui.cheng@caltech.edu), Christian Frankenberg (cfranken@caltech.edu)

Abstract. Photosynthesis by terrestrial plants represents the majority of [..[1]]CO_2 uptake on Earth, yet it is difficult to measure directly from space. [..[2]]Estimation of Gross Primary Production (GPP) from remote sensing indices [..[3]]represents a primary source of uncertainty, in particular for observing seasonal variations in evergreen forests. Recent vegetation remote sensing techniques have highlighted spectral regions sensitive to dynamic changes in leaf/needle carotenoid composition, showing promise for tracking seasonal changes in photosynthesis of evergreen forests. However, [..[4]]these have mostly been investigated with intermittent field campaigns, or with narrow-band spectrometers in these ecosystems. To investigate this potential, we continuously measured vegetation reflectance (400–900 nm) using a canopy spectrometer system, PhotoSpec, mounted on top of an eddy-covariance flux tower in a subalpine evergreen forest at Niwot Ridge, Colorado, USA. We analyzed driving spectral components in the measured canopy reflectance using both statistical and process-based approaches. The decomposed spectral components [..[5]]co-varied with carotenoid content and GPP, supporting the interpretation of the Photochemical Reflectance Index (PRI) and the Chlorophyll/Carotenoid Index (CCI). [..[6]]Although the entire 400-900 nm range [..[7]

[1]removed: CO2
[2]removed: Estimating
[3]removed: is
[4]removed: continuous daily measurements of spectrally resolved canopy reflectance are limited
[5]removed: relate directly to carotenoid pigments and co-vary seasonally with
[6]removed: We show that using features from
[7]removed: show

]showed additional spectral changes near the [..[8]]red-edge, it did not provide significant improvements in GPP predictions. We found little seasonal variation in both Normalized Difference Vegetation Index (NDVI) and the Near Infrared Vegetation Index (NIRv) in this ecosystem. In addition, we [..[9]]quantitatively determined needle-scale chlorophyll to carotenoid ratios as well as anthocyanin contents using full spectrum inversions, both of which were tightly correlated with seasonal GPP changes. Reconstructing GPP from vegetation reflectance using Partial Least Squares Regression (PLSR) explained approximately 87% of the variability in observed GPP. Our results [..[10]]linked the seasonal variation of reflectance to the pool size of photoprotective pigments, highlighting all spectral locations within 400–900 nm associated with GPP seasonality in evergreen forests.

1 Introduction

Terrestrial Gross Primary Production (GPP), the gross CO_2 uptake through photosynthesis, is the largest uptake of atmospheric CO_2 (Ciais et al., 2013), yet the uncertainties are large, hampering our ability to monitor and predict the response of the terrestrial biosphere to climate change (Ahlström et al., 2012). Hence, accurately mapping GPP globally is critical. In contrast to unevenly distributed ground-level measurements such as Fluxnet (Baldocchi et al., 2001), satellites can [..[11]]infer GPP globally and uniformly. Remote sensing techniques are based on the optical response of vegetation to incoming sunlight[..[12]], which can track photosynthesis via the absorption features of photosynthetic and photoprotective pigments (Rouse Jr et al., 1974; Liu and Huete, 1995; Gamon et al., 1992, 2016). [..[13]]Progress is particularly important for evergreen forests, which can have large seasonal dynamics in photosynthesis but low variability in canopy structure and color. However, these promising techniques still lack a comprehensive evaluation/validation using both continuous in-situ measurements as well as process-based simulations.

GPP can be expressed as a function of photosynthetically active radiation (PAR), the fraction of PAR absorbed by the canopy (fPAR) and Light-Use Efficiency (LUE):

$$[..^{14}]\mathrm{GPP} = [..^{15}]\mathrm{PAR} \cdot [..^{16}]\mathrm{fPAR} \cdot [..^{17}]\mathrm{LUE}, \quad (1)$$

with LUE representing the efficiency of plants to fix carbon using absorbed light (Monteith, 1972; Monteith and Moss, 1977). The accuracy of remote sensing derived GPP is limited by the estimation of LUE, which is more dynamic and difficult to measure remotely than PAR and fPAR, particularly in evergreen ecosystems. There have been [..[18]]many studies inferring the light absorbed by canopies (i.e. fPAR) from Vegetation Indices (VIs) that estimate the 'greenness' of canopies (Running et al., 2004; Zhao et al., 2005; Robinson et al., 2018; Glenn et al., 2008), such as the Normalized Difference Vegetation Index

[8] removed: red-egde but do not outperform the PRI or CCI indices for
[9] removed: can quantitatively determine
[10] removed: link
[11] removed: measure
[12] removed: . Remote sensing techniques have made progress on tracking photosynthesis using
[13] removed: The progress
[18] removed: several

(NDVI; Rouse Jr et al., 1974; Tucker, 1979), the Enhanced Vegetation Index (EVI; Liu and Huete, 1995; Huete et al., 1997) and the Near Infrared Vegetation Index (NIRv; Badgley et al., 2017). Current GPP data products derived from Eq. (1) rely on the modulation of abiotic conditions to estimate LUE (Xiao et al., 2004). LUE is derived empirically by defining a general timing of dormancy for all evergreen forests with the same plant functional type (e.g. Krinner et al., 2005) or the same meteorological thresholds (e.g. Running et al., 2004). However, within the same climate region or plant functional type, forests are not identical - leading to uncertainties in estimated LUE (Stylinski et al., 2002; Gamon et al., 2016; Zuromski et al., 2018), which propagate to the estimation of GPP.

[..[19]]Because evergreen trees retain most of their needles and chlorophyll throughout the entire year [..[20]](Bowling et al., 2018), LUE in evergreens is regulated by needle biochemistry. As LUE falls with the onset of winter due to unfavorable environmental conditions and seasonal downregulation of photosynthetic capacity, evergreen needles [..[21]]quench excess absorbed light via thermal energy dissipation that involves xanthophyll cycle and other pigments (Adams and Demmig-Adams, 1994; Demmig-Adams and Adams, 1996; Verhoeven et al., 1996; Zarter et al., 2006). Thermal energy dissipation is [..[22]]a primary de-excitation pathway measured by pulse-amplitude fluorescence as non-photochemical quenching (NPQ[..[23]]; Schreiber et al. (1986)). At the same time, a small amount of radiation, Solar-Induced Fluorescence (SIF), via the de-excitation of absorbed photons is emitted by photosystem II (Genty et al., 1989; Krause and Weis, 1991).

Some vegetation indices are sensitive to photoprotective pigments (e.g. carotenoids) and can characterize the seasonality of evergreen LUE with some success. For instance, the Photochemical Reflectance Index (PRI; Gamon et al., 1992, 1997) and Chlorophyll/Carotenoid Index (CCI; Gamon et al., 2016) both use wavelength regions that represent carotenoid absorption features around 531 nm at the leaf level (Wong et al., 2019; Wong and Gamon, 2015a, b) and show great promise for estimating photosynthetic seasonality (Hall et al., 2008; Hilker et al., 2011a). [..[24]]Due to the relatively invariant canopy structure in evergreen forests, CCI and PRI have been applied at the canopy level as well (Gamon et al., 2016; Garbulsky et al., 2011; Middleton et al., 2016). In addition, the [..[25]]Green Chromatic Coordinate (GCC; Richardson et al., 2009, 2018; Sonnentag et al., 2012), an index derived from [..[26]]the brightness levels of RGB canopy images, is also capable of tracking the seasonality of evergreen GPP (Bowling et al., 2018). However, the full potential of spectrally resolved reflectance measurements to explore the photosynthetic phenology of evergreens has not been comprehensively explored at the canopy scale. The evaluation of [..[27]]pigment-driven spectral changes in evergreen forests over the course of a season is necessary to [..[28]]determine where, when,

[19] removed: LUE in evergreen forests is regulated not only by abiotic conditions, but also biotic processes. Unlike deciduous forests, evergreen trees keep

[20] removed: . Seasonal GPP variations in evergreens are thus driven by LUE (Bowling et al., 2018). In order to regulate LUE

[21] removed: have to quench the excess absorbed sunlight through non-photochemical pathways - i.e. regulating the pool size of pigments involved in the dissipation of excess light , the xanthophyll cycle pigments (Adams and Demmig-Adams, 1994; Demmig-Adams and Adams, 1996; Zarter et al., 2006), among other pigments (Verhoeven et al., 1996). While the regulation of excess

[22] removed: often done through several mechanisms, these pathways are summarized under the term

[23] removed:).

[24] removed: Because of the stable

[25] removed: green chromatic coordinate

[26] removed: red-green-blue

[27] removed: pigment driven

[28] removed: evaluate

and why certain wavelength regions could advance our mechanistic understanding of canopy photosynthetic and photoprotective pigments. However, this has not been done with both empirical and process-based methods using continuously measured canopy hyperspectral reflectance and in situ pigment samples.

Here, we [..[29]]used continuous measurements in both spectral space (full spectrum between 400–900 nm) and time ([..[30]]daily over an entire year) to evaluate the potential of hyperspectral canopy reflectance for better understanding [..[31]]the sensitivity of VIs to pigment changes that regulate GPP in evergreen forests. Continuous measurements of spectrally resolved reflectance at the canopy scale have so far been sparse at evergreen forest sites [..[32]](Gamon et al., 2006; Hilker et al., 2011b; Porcar-Castell et al., 2015; Rautiainen et al., 2018; Wong et al., 2020). There are only a few empirical studies on hyperspectral canopy reflectance in evergreen forests (Smith et al., 2002; Singh et al., 2015). Yet, empirically decomposed canopy spectral reflectance has been used as a predictor of maximum photosynthetic capacity (Serbin et al., 2012; Barnes et al., 2017; Dechant et al., 2017; Silva-Perez et al., 2018; Meacham-Hensold et al., 2019), GPP (Matthes et al., 2015; Huemmrich et al., 2017; DuBois et al., 2018; Huemmrich et al., 2019; Dechant et al., 2019), and other physiological properties (Ustin et al., 2004, 2009; Asner et al., 2011; Serbin et al., 2014).

In contrast to empirical methods, process-based approaches, such as canopy Radiative Transfer Models (RTMs) can help to quantitatively link canopy photosynthesis with leaf-level contents of photosynthetic/photoprotective pigments (Feret et al., 2008; Jacquemoud et al., 2009). With RTMs, we can use spectrally resolved reflectance to directly derive leaf pigment contents (Féret et al., 2017; Jacquemoud et al., 1995) and plant traits (Féret et al., 2019) .

[..[33]]In addition to seasonal changes in pigment concentrations, canopy SIF was found to correlate significantly with the seasonality of photoprotective pigment content in a subalpine coniferous forest (Magney et al., 2019). Steady state SIF is regulated by NPQ and photochemistry (Porcar-Castell et al., 2014)[..[34]], and it provides complementary information on canopy GPP. [..[35]]Yang and van der Tol (2018) justified that the relative SIF, SIF normalized by the reflected near-infrared radiation, is more representative of the physiological variations of SIF as it is comparable to a SIF yield (Guanter et al., 2014; Genty et al., 1989). Our continuous optical measurements make it possible to differentiate mechanisms undergoing seasonal changes by comparing the decomposed reflectance spectrum against relative far-red SIF. Additionally, using relative SIF can effectively correct for incoming irradiance and account for the sunlit/shade fraction within the observation Field of View (FOV) of PhotoSpec (Magney et al., 2019).

[29] removed: use

[30] removed: sub-daily

[31] removed: VIs sensitive

[32] removed: (Gamon et al., 2006; Hilker et al., 2011b; Porcar-Castell et al., 2015; Rautiainen et al., 2018)

[33] removed: Continuously observed reflectance makes it possible to differentiate NPQ pathways by comparing the methods mentioned above and VIs against far-red Solar-Induced Fluorescence (SIF), which is also available from our canopy spectrometer system, PhotoSpec (Grossmann et al., 2018). SIF is a very small amount of radiation, relative to reflectance, released via the de-excitation of absorbed photons by photosystem II (Genty et al., 1989; Krause and Weis, 1991)

[34] removed: and

[35] removed: Magney et al. (2019) found the seasonality of photoprotective pigment content in a subalpine coniferous forest is significantly correlated with canopy SIF .

In the present study, we [..[36]]analyzed continuous canopy reflectance data from PhotoSpec at a subalpine evergreen forest at the Niwot Ridge AmeriFlux site (US-NR1) in Colorado, US, and [..[37]]sought to understand the mechanisms controlling the seasonality of photosynthesis using continuous hyperspectral remote sensing. We first [..[38]]explored empirical techniques to study all seasonal variations in reflectance spectra, [..[39]]identified specific spectral regions that best [..[40]]explained the seasonal changes in GPP, and then [..[41]]linked these spectral features to pigment absorption features that [..[42]]impacted both biochemical and biophysical traits. We also [..[43]]used full spectral inversions using a canopy RTM to infer quantitative estimates of leaf pigment pool sizes. Finally, we [..[44]]compared the spring onset of photosynthesis captured by different methods[..[45]], VIs, and relative SIF to determine the underlying mechanisms [..[46]]that contributed to photosynthetic phenology.

2 Material and methods

2.1 Study site

The high-altitude (3050 m above sea level) subalpine evergreen forest near Niwot Ridge, Colorado, US, is an active AmeriFlux site (US-NR1, Lat: 40.0329 °N, Lon: 105.5464 °W; tower height: 26 m; Monson et al., 2002; Burns et al., 2015, 2016; Blanken et al., 2019). Three species dominate: subalpine fir (*Abies lasiocarpa var. bifolia*), Englemann spruce (*Picea engelmannii*), and lodgepole pine (*Pinus contorta*) with an average height of 11.5 m, a leaf area index of 4.2 (Burns et al., 2016), and minimal understory. The annual mean precipitation and air temperature are 800 mm and 1.5 °C, respectively (Monson et al., 2002). The high elevation creates an environment with cold winters (with snow present more than half the year), while the relatively low latitude (40°N) allows for year-round high solar irradiation (Monson et al., 2002). Thus, trees have to dissipate a considerable amount of excess sunlight during [..[47]]winter dormancy, which makes this forest an ideal site for studying seasonal variation of NPQ including the sustained component of it during dormancy (Bowling et al., 2018; Magney et al., 2019).

2.2 Continuous tower-based measurements of canopy reflectance

PhotoSpec (Grossmann et al., 2018) is a 2D scanning telescope spectrometer unit originally designed to measure SIF. It also features a broad-band Flame-S spectrometer (Ocean Optics, Inc., Florida, USA), used to measure reflectance from 400 to

[36] removed: analyze
[37] removed: seek
[38] removed: explore
[39] removed: identify
[40] removed: explain
[41] removed: link
[42] removed: impact
[43] removed: use
[44] removed: compare
[45] removed: and VIs
[46] removed: of the methods/VIs that contribute
[47] removed: the

900 nm at a moderate (full-width-at-half-maximum = 1.2 nm) spectral resolution with a [..[48]]FOV of 0.7° (more details in Grossmann et al. (2018); Magney et al. (2019)). In the summer of 2017, we installed a PhotoSpec system on the top of the US-NR1 eddy-covariance tower, from where we can scan the canopy by changing both viewing azimuth angle and zenith angles. On every other summer day and every winter day, PhotoSpec scans the canopy by changing [..[49]]view zenith angle with small increments at fixed view azimuth angles, i.e. elevation scans. Only one azimuth position is kept after Oct 18, 2017 to protect the mechanism from potentially damaging winter conditions at the site. Spectrally resolved reflectance was calculated using direct solar irradiance measurements via a cosine diffuser mounted in the upward nadir direction (Grossmann et al., 2018) as well as reflected radiance from the canopy. The reflectance data used in this study are from Jun 16, 2017, to Jun 15, 2018.

Here, we integrated all elevation scans to daily-averaged [..[50]]reflectance (every other day before Oct 18, 2017) by using all scanning viewing directions with vegetation in the field of view over the course of a day, filtering for both low light conditions and thick clouds by requiring PAR to be both at least 100 μmol $m^{-2}s^{-1}$ and 60% of theoretical clear-sky PAR. A detailed description of data processing can be found in appendix B. To further test whether bi-directional reflectance effects impacted our daily averages, we compared the NDVI and NIRv at various canopy positions given a range of solar zenith and azimuth angles ([..[51]]Fig. A1-3). Neither of the daily averaged VIs was substantially impacted by the solar geometry supporting the robustness of daily averaged canopy reflectance. An additional analysis (Fig. A4) has also shown the variation in phase angle at a daily time step is not a critical factor for the change in reflectance.

About 49 winter days exhibited significantly higher reflectances, attributable to snow within the field of view, which we corroborated with canopy RGB imagery from the tower. After removing data strongly affected by snow and excluding the days of instrument outages, 211 valid sample days remained, among which 96 valid sample days were between DOY 100-300. The daily-averaged reflectance was computed as the median reflectance from all selected scans for a single day, which was then smoothed by a 10-point (3.7 nm) box-car filter over the spectral dimension (400 - 900 nm) to remove the noise in the spectra. Figure 1(a) shows the seasonally averaged and spectrally resolved canopy reflectances measured by PhotoSpec.

[48] removed: field of view (FOV)
[49] removed: the
[50] removed: reflectances
[51] removed: appendix A1

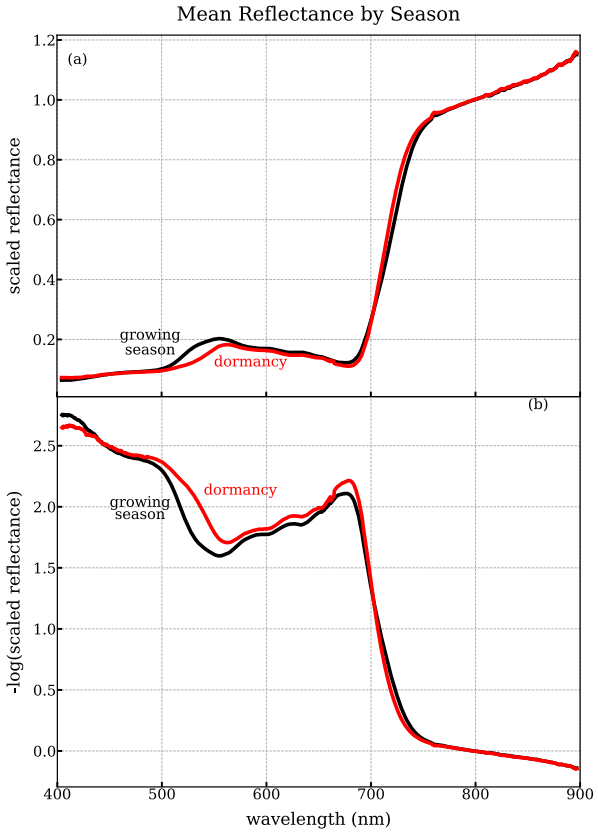

Figure 1. (a) Seasonally averaged canopy reflectance in winter dormancy (red) and the growing season (black) from PhotoSpec. (b) Seasonally averaged negative logarithm transformation of reflectance (400 - 900 nm). For comparison, we normalized the reflectance by the value at 800 nm on each day. Here, we [..[52]]referred to Nov 13 - Apr 18 as dormancy, and Jun 2 - Aug 21 [..[53]]as the main growing season. The seasonal averaged canopy reflectance is composed of 39 daily-average reflectance in the growing season and 113 daily-averaged reflectance in the dormancy.

To further emphasize the change in reflectance as a result of changes in pigment contents, we transformed the reflectance (shown as [..[54]]R_λ) using the negative logarithm (Eq. (2)), as light intensity diminishes exponentially with pigment contents (Horler et al., 1983).

$$R_\lambda \propto exp(-C \cdot \sigma(\lambda)) \tag{2a}$$

$$C \cdot \sigma(\lambda) \propto -log(R_\lambda) \tag{2b}$$

with $\sigma =$ absorption cross section of pigments.

[54]removed: R_λ

Therefore, the log-transformed reflectance (Fig. 1(b)) should correlate more linearly with pigment contents (shown as [..[55]]C). We also considered a variety of typical VIs using the reflectance data from PhotoSpec, such as:

$$[..^{56}]\text{NDVI} = \frac{R_{800} - R_{670}}{R_{800} + R_{670}} \text{ (Rouse Jr et al., 1974)} \tag{3a}$$

$$[..^{57}]\text{NIRv} = [..^{58}]\text{NDVI} * \text{R}_{800} \text{ (Badgley et al., 2017)} \tag{3b}$$

$$[..^{59}]\text{PRI} = [..^{60}]\frac{\text{R}_{531} - \text{R}_{570}}{\text{R}_{531} + \text{R}_{570}} \text{ (Gamon et al., 1992)} \tag{3c}$$

$$[..^{61}]\text{CCI} = \frac{R_{526-536} - R_{620-670}}{R_{526-536} + R_{620-670}} \text{ (Gamon et al., 2016)} \tag{3d}$$

$$[..^{62}]\text{GCC} = \frac{R_{Green}}{R_{Red} + R_{Green} + R_{Blue}} \text{ (Richardson et al., 2009).} \tag{3e}$$

In order to calculate GCC, we convolved the reflectance using the instrumental spectral response function (Fig. S1; Wingate et al., 2015) of the StarDot NetCam SC 5 MP IR (StarDot Technologies, Buena Park, CA, USA), which is the standard camera model [..[63]]used by the PhenoCam Network protocol (Sonnentag et al., 2012).

In addition to the reflectance measurments, we also included relative SIF[..[64]], far-red SIF normalized by the reflected [..[65]]near-infrared radiance at 755 nm. The far-red SIF (745–758 nm, Grossmann et al., 2018) was measured simultaneously with reflectance with a QEPro spectrometer (Ocean Optics, Inc., Florida, USA). The daily relative SIF was processed in the same fashion as the reflectance.

2.3 Eddy covariance measurements and LUE

[..[66]]

Observations of Net Ecosystem Exchange (net flux of CO_2, NEE), PAR, and meteorological variables made at the US-NR1 tower are part of the official AmeriFlux Network data (Burns et al., 2016). GPP was estimated in half-hourly intervals (Reichstein et al., 2005) using the REddyProc package (Wutzler et al., 2018), allowing us to compute LUE (Goulden et al., 1996; Gamon et al., 2016) at half-hourly intervals.

[..[67]]According to the light response curves[..[68]], GPP is a nonlinear function of PAR (Fig. 2; Harbinson, 2012). Magney et al. (2019) showed that fPAR does not significantly vary with seasons. [..[69]]We started to observe a photosynthetic saturation between 500-1000 μmol $m^{-2}s^{-1}$ of PAR (Fig. 2), when the carboxylation rate, driven by maximum carboxylation

[55] removed: C

[63] removed: prescribed

[64] removed: as well. Yang and van der Tol (2018) justified that the relative SIF,

[65] removed: radiation, is more representative for the physiological variations of SIF since it accounts for the complexity of signal due to canopy structure.

[66] removed: An array of up and down-looking PAR sensors (SQ-500-SS; Apogee Instruments, Utah, US) above and below the canopy was used to calculate fPAR in half-hourly intervals. fPAR was smoothed with an 8-point (4 hour) running mean and 20-day running mean to remove the noise in the measurements.The first fPAR measurement started on Aug 8, 2017 (DOY 220).

[67] removed: The

[68] removed: show that

[69] removed: At high light intensity,

rate (V[..[70]]$_{cmax}$), became the limiting factor (Farquhar et al., 1980). Thus, we defined the [..[71]]light-saturated GPP (GPP$_{max}$), as the mean half-hourly GPP at PAR levels between 1000 and 1500 μmol $m^{-2}s^{-1}$, a range which [..[72]]was covered throughout the year (Fig. 2), even in winter. Therefore, GPP$_{max}$ [..[73]]was less susceptible to short term changes in PAR. Yet, [..[74]]due to the lower light intensity during storms, GPP$_{max}$ was not always available. As suggested by the low PAR value at which light saturation happened, plants remained in a light saturated condition for most of the daytime. A higher GPP$_{max}$ [..[75]]indicates a greater V[..[76]]$_{cmax}$ and maximum electron transport rate (J$_{max}$) when the variation of GPP$_{max}$ is independent from stomatal conductance and intercellular CO_2 concentration (Leuning, 1995). [..[77]][..[78]]Therefore, GPP[..[79]]$_{max}$ was closely correlated with daily LUE driven by physiology (see section 2.4 in the supplementary material).

We refrained from normalizing GPP$_{max}$ by APAR due to some of APAR measurements (see section 2.1 in the supplementary material) not available in the beginning of growing season. GPP$_{max}$ was significantly linearly correlated with normalized GPP$_{max}$ by APAR (Fig. S2c).

We also included [..[80]]Air Temperature (T$_{air}$) and Vapor Pressure Deficit (VPD) provided from the AmeriFlux network data. Daytime daily mean T$_{air}$ and VPD were [..[81]]computed from averaging the half-hourly T$_{air}$ and VPD when PAR was greater than 100 μmol $m^{-2}s^{-1}$.

[70] removed: $_{cmax}$), becomes

[71] removed: high-light/

[72] removed: is

[73] removed: is

[74] removed: GPP$_{max}$ is proportional to V$_{cmax}$ when the carboxylation rate limits photosynthesis

[75] removed: thus

[76] removed: $_{cmax}$

[77] removed: At low light intensity, photosynthesis is light limited. To implement Eq.

[78] removed: , we defined the light limited LUE (LUE$_{lightL}$) as the fitted slope of APAR against GPP at PAR between 100 and 500 μmol $m^{-2}s^{-1}$. We calculated GPP$_{max}$ and LUE$_{lightL}$ from half-hourly GPPand APAR for each day. We also defined a more generalized effective daily LUE (LUE$_{total}$) as the daily averaged ratio of

[79] removed: to APAR during the day. This effective daily LUE would be most applicable for empirical LUE models that work on daily time-steps

[80] removed: the meteorological variables provided from the AmeriFlux network data, such as

[81] removed: extracted from

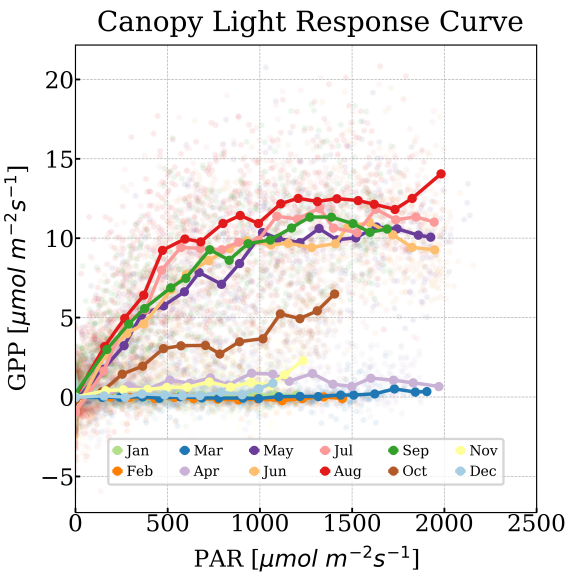

Figure 2. Half-hourly GPP as a function of PAR during the measurement period. Points [..[82]]were colored by month. Bold points [..[83]]were the median GPP when PAR [..[84]]was binned every 100 μmol $m^{-2}s^{-1}$ approximately. The solid lines represent the canopy light response curve.

2.4 Pigment measurements

To link canopy reflectance with variations in pigment contents, we used pigment data (Bowling et al., 2018; Bowling and Logan, 2019; Magney et al., 2019) at monthly intervals over the course of the sampling period. Here, we focused on the [..[85]]xanthophyll cycle pool size (Violaxanthin + Antheraxanthin + Zeaxanthin, V+A+Z)[..[86]], total carotenoid content ([..[87]]car) and total chlorophyll content (chl) measured on *Pinus contorta* and *Picea engelmannii* needles with units of moles per unit fresh mass. [..[88]]car includes V+A+Z, lutein, neoxanthin, and beta-carotene. We also [..[89]]computed the ratio of chlorophyll to carotenoid contents ([..[90]]chl:car), because CCI derived from Moderate Resolution Imaging Spectroradiometer (MODIS) can track chl:car (Gamon et al., 2016). Overall, we can match 10 individual leaf-level sampling days for both pine and spruce samples with reflectance measured within $\pm$ 2 days. Among these 10 valid sample days, 6 sample days are between DOY 100-300.

[85] removed: total xanthophyll content
[86] removed: and
[87] removed: *car*)
[88] removed: *car*
[89] removed: compute
[90] removed: *chl:car*

2.5 Data-driven spectral decomposition

We [..[91]]assumed that the spectrally resolved reflectance is a result of mixed absorption processes by different pigments. This [..[92]]allowed us to apply an Independent Component Analysis (ICA; Hyvärinen and Oja, 2000) to decompose the log-transformed reflectance matrix (day of the year in rows and spectral dimension in columns) into its independent components. An advantage of the ICA is that it can separate a multivariate signal into additive subcomponents that are maximally independent, without the condition of orthogonality (Comon, 1994). [..[93]]We extracted three independent components, which explained more than 99.99% of the variance, using the ICA algorithm (fastICA, python package scikit-learn v0.21.0[..[94]]; section 4 in the supplementary material), such as:

$$-\log(R_{\lambda,DOY}) = \sum_{i=1,2,3} (\text{spectral component}^{i}_{\lambda} \cdot \text{temporal loading}^{i}_{DOY}). \quad (4)$$

where i is the i'th component in spectral space.

The decomposed spectral components revealed characteristic features that explain most of the variance in the reflectance matrix, which dictated the time-independent spectral shapes of pigment absorption features [..[95]]based on Eq. (2). The corresponding temporal loadings showed temporal variations of these spectral features, i.e. the variations of pigment contents. We will introduce the method of extracting pigment absorption features in a quantitative model-driven approach in section 2.6.

In addition to analyzing the transformed reflectance alone, we empirically correlated the reflectance with [..[96]]GPP_{max} using Partial Least Squares Regression (PLSR, python package scikit-learn v0.21.0). PLSR is a predictive regression model which solves for a coefficient that can maximally explain the linear covariance of the predictor with multiple variables (Wold et al., 1984; Geladi and Kowalski, 1986). [..[97]]PLSR has been used to successfully predict photosynthetic properties using reflectance matrices in previous studies from the leaf to canopy scales (e.g. Serbin et al., 2012, 2015; Barnes et al., 2017; Silva-Perez et al., 2018; Woodgate et al., 2019). [..[98]]Applying the PLSR to the hyperspectral canopy reflectance and GPP_{max} resulted in a time-independent coefficient that emphasizes the key wavelength regions which contribute to the covariation of reflectance and GPP_{max}, such as:

$$GPP_{max,DOY} = -\log(R_{\lambda,DOY}) \times \text{PLSR coefficient}^{GPP_{max}}_{\lambda}. \quad (5)$$

[91] removed: assume

[92] removed: allows

[93] removed: The decomposed spectral components reveal characteristic features that explain most of the variance in the reflectance matrix. The corresponding temporal components show temporal variations of these spectral features.

[94] removed:), which explain more than 99.99% of the variance. The set of independent (spectral) components contain

[95] removed: , which suggests that the corresponding temporal components are related to

[96] removed: LUEs/

[97] removed: Applying the PLSR on the hyperspectral canopy reflectance and LUEs/GPP_{max} results in a coefficient that emphasizes the key wavelength regions that contribute to the covariation. PLSR

[98] removed: We used four PLSR components based on a four-fold cross-validation.

We implemented another set of PLSR analyses on the reflectance with individual pigment measurement as the target variable, such as the mean values of V+A+Z, car, and chl:car[..[99]], such as:

$$\text{pigment measurement} = -\log(R_{\lambda,\text{DOY}}) \times \text{PLSR coefficient}_{\lambda}^{\text{pigment measurement}}. \quad (6)$$

We did not include chl as one of the target variables in this PLSR analysis since Bowling et al. (2018) and Magney et al. (2019) have already shown chl did not vary seasonally in our study site. Fitting the minimal variance in chl will lead to over fitting the PLSR model.

Comparing the PLSR coefficient of pigment measurements at the leaf level with the PLSR coefficient of [..[100]]GPP_{max} connected the changes in [..[101]]GPP_{max} to the pool size of [..[102]]photoprotective pigments, because the reflectance is regulated by the absorption of pigments.

2.6 Process-based methods

PROSPECT+SAIL (PROSAIL, Jacquemoud et al., 2009) is a process-based 1-D canopy [..[103]]RTM that models canopy reflectance, given canopy structure information (SAIL) as well as leaf pigment contents (PROSPECT) (Jacquemoud and Baret, 1990; Vilfan et al., 2018).

We [..[104]]used PROSAIL (with PROSPECT-D, Féret et al., 2017) to compute the derivative of the daily-averaged negative logarithm transformed reflectance with respect to individual pigment contents, namely chlorophyll content (chlorophyll Jacobian, [..[105]]$\frac{\partial -log(R)}{\partial C_{chl}}$) and carotenoid content (carotenoid Jacobian, [..[106]]$\frac{\partial -log(R)}{\partial C_{car}}$) (Dutta et al., 2019). This helped explain the decomposed spectral components from the empirical analysis.

We also [..[107]]used PROSAIL to infer pigment contents (i.e. C_{chl}, C_{car}, C_{ant}) by optimizing the agreement between PROSAIL-modeled reflectance and measured canopy daily-mean reflectance from PhotoSpec. We fixed canopy structural parameters (e.g. the LAI to 4.2, as reported in Burns et al. (2015)) and fitted leaf pigment compositions as well as a low order polynomial for soil reflectance (appendix C), similar to Vilfan et al. (2018) and Féret et al. (2017). The cost function J in Eq. (7) represents a least-squares approach, where $\hat{R}$ is the modeled reflectance.

$$[..^{108}]\text{J} = \sum_{\lambda=450nm}^{800nm} (R_\lambda - \hat{R}_\lambda)^2. \quad (7)$$

We used the spectral range between 450 and 800 nm, which encompasses most pigment absorption features.

[99] removed: . We used a leave-one-out cross-validation because of the small sample size and found that two PLS components are optimal.
[100] removed: LUEs/GPP_{max} connects
[101] removed: LUEs/
[102] removed: V+A+Z
[103] removed: radiative transfer model (RTM)
[104] removed: use
[105] removed: $\frac{\partial -log(R)}{\partial Cchl}$
[106] removed: $\frac{\partial -log(R)}{\partial Ccar}$) . This helps explain the variations in reflectance decomposed
[107] removed: use

3 Results and discussion

3.1 Seasonal cycle of GPP_{max} and environmental conditions

[..[109]]As can be seen in Fig. 3, the subalpine evergreen forest at Niwot Ridge exhibits strong seasonal variation in GPP, T_{air}, VPD, GPP_{max}, and PAR[..[110]]. GPP and $GPP_{[..[111]]max}$ [..[112]]dropped to zero while sufficient PAR, required for photosynthesis, was still available in the dormancy, which suggests that the abiotic environmental factors impact photosynthesis seasonality nonlinearly and jointly.

[..[113]][..[114]]Abiotic factors played a strong role in regulating GPP_{max} in this subalpine evergreen forest over the course of the season. For instance, [..[115]]there was a strong dependence of GPP_{max} with T[..[116]]$_{air}$. However, photosynthesis completely shut down during dormancy, even when the [..[117]]T_{air} exceeded 5°C [..[118]](Fig. 3). During the onset and cessation periods of photosynthesis, GPP_{max} rapidly [..[119]]increased with temperature (Fig. S3a left panel), potentially because needle temperature [..[120]]co-varied with T_{air}, and needle temperature controls the activity of photosynthetic enzymes which [..[121]]affect V_{cmax}. Spring warming approaches the optimal temperature for photosynthetic enzymes, leading to activation of photosynthesis, while cooling in the early winter inhibits these enzymes (Rook, 1969). Warming in spring melted frozen boles and made them available for water uptake (Bowling et al., 2018), and thus caused the recovery of GPP_{max} (Monson et al., 2005). Once the temperature [..[122]]was around the optimum (in the growing season), T_{air} [..[123]]was no longer the determining factor for photosynthesis. [..[124]]Higher VPD caused by rising T_{air} can stress the plants such that stomata closed, intercellular

[109] removed: The

[110] removed: (which is still sufficiently high to drive photosynthesis in winter)(Fig. 3 and Fig. S2). Needles use light most efficiently at low light levels (LUE

[112] removed:) for a fraction of the day. We start to observe a photosynthetic saturation at low PARvalues (~ 500 μmol $m^{-2}s^{-1}$; Fig. 2), which is represented by GPP_{max}, resulting in low efficiencies under high light conditions. LUE_{total} represents the mean light use scheme throughout the day. Hence, LUE_{light} was slightly higher than LUE_{total} during most of the growing season (Fig. S2). There were only a few days when PAR is so low that LUE did not reach light saturation for most of the day, when LUE_{total} is more comparable to LUE_{light}. Therefore, we only show the results of GPP_{max} in the rest of our analysis in the main text as it is more representative than LUE_{lightL} and more physiology-driven than LUE_{total}. In addition, LUE_{lightL} and LUE_{total} have more missing data than GPP_{max}. Yet, due to the lower light intensity during storms, GPP_{max} is not always available.

[113] removed: Time series of Air Temperature (T_{air}), Vapor Pressure Deficit (VPD), Photosynthetically Active Radiation (PAR), Gross Primary Production (GPP), and GPP_{max}. DOY 166 (2017) is the first day of observation. The vertical dashed line divides the observations from Day of Year (DOY) for year 2017 and 2018.

[114] removed: Abiotic factors play

[115] removed: as can be seen in Fig. S3, there is

[116] removed: , with an almost complete shutdown of photosynthesis

[117] removed: air temperature exceeds

[118] removed: . During periods at

[119] removed: increases with temperature

[120] removed: co-varies

[121] removed: affects V_{cmax}

[122] removed: is

[123] removed: is

[124] removed: Melting snow with warming in spring made soil water available for uptake and caused the recovery of GPP_{max} (Monson et al., 2005).

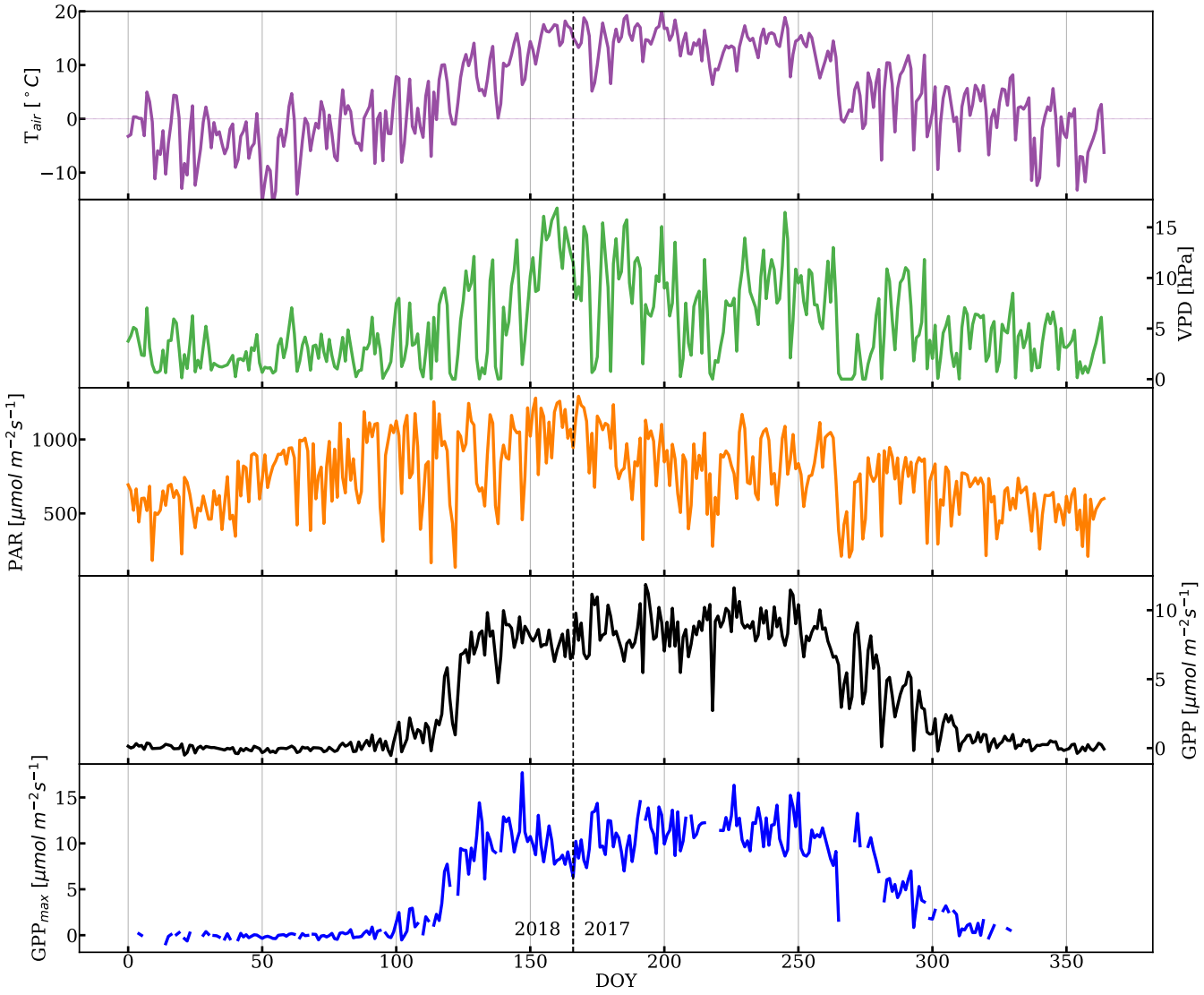

Figure 3. Daily-averaged time series of Air Temperature (T_{air}), Vapor Pressure Deficit (VPD), Photosynthetically Active Radiation (PAR), Gross Primary Production (GPP) from half-hourly data when PAR was greater than 100 μmol $m^{-2}s^{-1}$, and time series of GPP_{max}. DOY 166 (2017) was the first day of observation. The vertical dashed line divides the observations from Day of Year (DOY) for year 2017 and 2018.

CO_2 reduced and photosynthesis decreased (Fig. S3a right panel). When intercellular CO_2 concentration [..[125]]was not a limiting factor, GPP_{max} [..[126]]was more representative of [..[127]]V_{cmax} and did not vary T significantly.

[125]removed: is

[126]removed: is

[127]removed: Vcmax and does not vary with PAR and

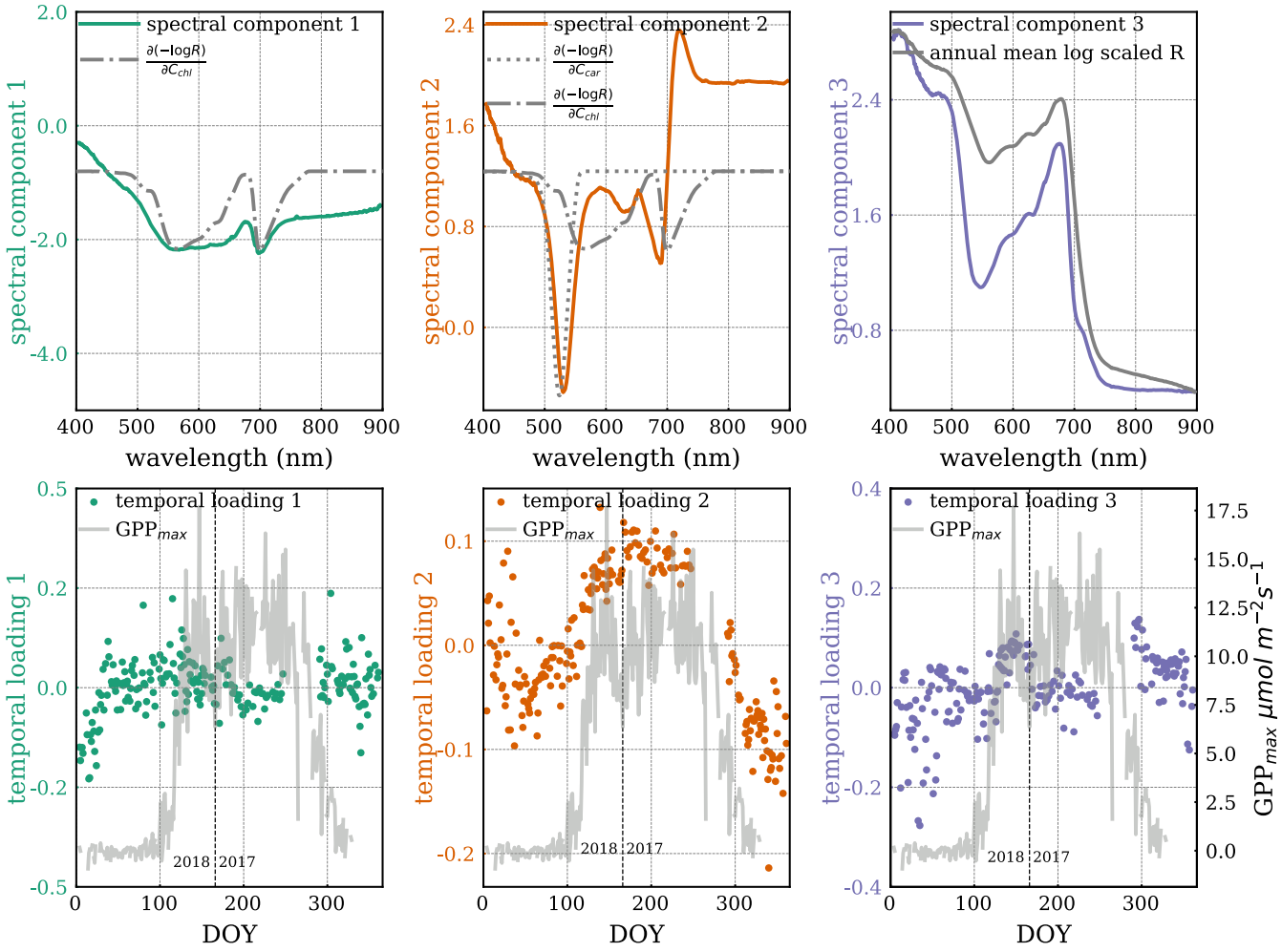

Figure 4. A set of three spectral components (top, colored) and corresponding temporal [..[128]]loadings (bottom, colored) from ICA decomposition. The first [..[129]]spectral [..[130]]component is overlaid with the chlorophyll Jacobian ([..[131]]$\frac{\partial -log(R)}{\partial C_{chl}}$, dash-dotted), and the second spectral component is overlaid with the carotenoid Jacobian ([..[132]]$\frac{\partial -log(R)}{\partial C_{car}}$, dotted). The third spectral component is overlaid on the annual mean shape of transformed reflectance spectra. Temporal [..[133]]loadings are overlaid with GPP_{max} (grey line). The axis of Jacobians is not shown because its magnitude is arbitrary here. The vertical dashed line divides the observations from DOY for year 2017 and 2018.

3.2 Seasonal cycle of reflectance

In Fig. 4, the Jacobians show the maximum sensitivity of the reflectance spectral shape to carotenoid content at 524 nm, and near 566 nm and 700 nm for chlorophyll. The first peak of the chlorophyll Jacobian covers a wide spectral range in the visible, while the second peak around the red edge is narrower.

It can be seen that the first spectral ICA component has a similar shape as the chlorophyll Jacobian. The corresponding temporal [..[134]]loading has a range between -0.2 to 0.2 without any obvious seasonal variation, consistent with a negligible seasonal cycle in chlorophyll content as shown in the pigment analysis. However, there is a gradual increase before DOY 50 in the first temporal [..[135]]loading, which appears to be anti-correlated with the temporal [..[136]]loading of the second ICA structure.

Two major features in the second spectral component can be observed. One is a negative peak centered around 530 nm, which aligns with the carotenoid Jacobian. At the negative logarithm scale, the negative values resulting from the negative ICA spectral peak multiplied by the positive ICA temporal [..[137]]loadings (growing season in Fig. 4 middle plots) indicate there were fewer carotenoids during the growing season [..[138]](Eq. (2) and Eq. (4)). Conversely, positive values resulting from a negative spectral peak multiplied by the negative temporal [..[139]]loadings (dormancy in Fig. 4 middle plots) indicate there were more carotenoids during dormancy (i.e. sustained photoprotection via the xanthophyll pigments; Bowling et al., 2018). Another feature [..[140]]is the valley-trough shape, which is co-located with the chlorophyll Jacobian center at the longer wavelength [..[141]]in the red-edge region. The center of this feature occurs at the shorter-wavelength edge of the chlorophyll Jacobian but does not easily explain changes in total chlorophyll content, which should show equal changes around 600 nm. The corresponding temporal [..[142]]loading apparently varied seasonally with GPP_{max}. [..[143]]

The second temporal loading transitioned more gradually from dormancy to the peak growing season than GPP_{max}. Unfortunately, we [..[144]]were missing data to evaluate the relative timing of GPP_{max} cessation.

The third spectral component is similar to the mean shape of reflectance spectra. Its temporal [..[145]]loading held around zero throughout the year.

Overall, the second ICA spectral component is more representative of the seasonal variation in the magnitude of total canopy reflectance than the other spectral components. The spectral changes around the red-edge in the second component is interesting and might be related to structural needle changes in chlorophyll-a and chlorophyll-b contributions (de Tomás Marín et al., 2016; Rautiainen et al., 2018), which are not separated in PROSPECT.

CCI [..[146]]and PRI(Fig. 5([..[147]]a-b)) followed the seasonal cycle of GPP_{max} closely. CCI and PRI use reflectance near the center of the 530 nm valley feature (Eq. (3)c-d), the spectral range that is most sensitive to the change of carotenoid content,

[134]removed: component
[135]removed: component
[136]removed: component
[137]removed: components indicate there are
[138]removed: .
[139]removed: components indicate there are
[140]removed: has a
[141]removed: at
[142]removed: component apparently varies
[143]removed: In addition, the second temporal component transitions
[144]removed: are
[145]removed: component holds
[146]removed: , PRI, and GCC
[147]removed: a-c)) follow

so that they [..[148]]matched changes in GPP_{max} very well. PRI [..[149]]was the smoothest throughout the year, without any
285 significant fluctuations within the growing season, as [..[150]]opposite to what was observed in GPP_{max}, which co-varied with T_{air} and VPD [..[151]](Fig. S3a and S3b). This performance is [..[152]]intriguing given that PRI was originally developed to track short term [..[153]]variations in LUE (Gamon et al., 1992)[..[154]], such as day-to-day and sub-seasonal scales.

GCC (Fig. 5(c)) also correlated well with GPP_{max}, but less than CCI and PRI. As can be seen in Fig. S1, the peak of the green channel used for GCC is close to the carotenoid Jacobian peak, while the red channel feature covers a part of
290 chlorophyll Jacobian feature. This [..[155]]explained the sensitivity of the GCC to changes in both carotenoid content as well as chlorophyll. The bands used in GCC [..[156]]are broader than the ones used by PRI and CCI, however it still [..[157]]captured these variations and can be computed using RGB imagery. Gentine and Alemohammad (2018) found that the green band helps to reconstruct variations in SIF using reflectances from MODIS. While they speculated that most variations in SIF are [..[158]]related to variations in [..[159]]PAR · fPAR (Gentine and Alemohammad, 2018), we [..[160]]suggest here that the green band
295 indeed captures variations in LUE as well.

NDVI (Fig. 5(e)) and NIRv (Fig. 5(f)) [..[161]]did not show an obvious seasonal variability.

Similar to the ICA components, all VIs [..[162]]were quite noisy during dormancy[..[163]], especially prior to DOY 50. This noise may be due to snow because we only removed the reflectance when the canopy was snow covered. Scattered photons possibly still reached the telescope when there was snow [..[164]]on the ground, which is true for our study site as snowpack
300 [..[165]]exists in winter (Bowling et al., 2018).

[148]removed: match
[149]removed: is
[150]removed: is
[151]removed: .
[152]removed: excellent
[153]removed: variation
[154]removed: . The GCC also correlates
[155]removed: explains
[156]removed: uses
[157]removed: captures
[158]removed: thus
[159]removed: $PAR \cdot fPAR$
[160]removed: show
[161]removed: do not have
[162]removed: are
[163]removed: .
[164]removed: at
[165]removed: commonly

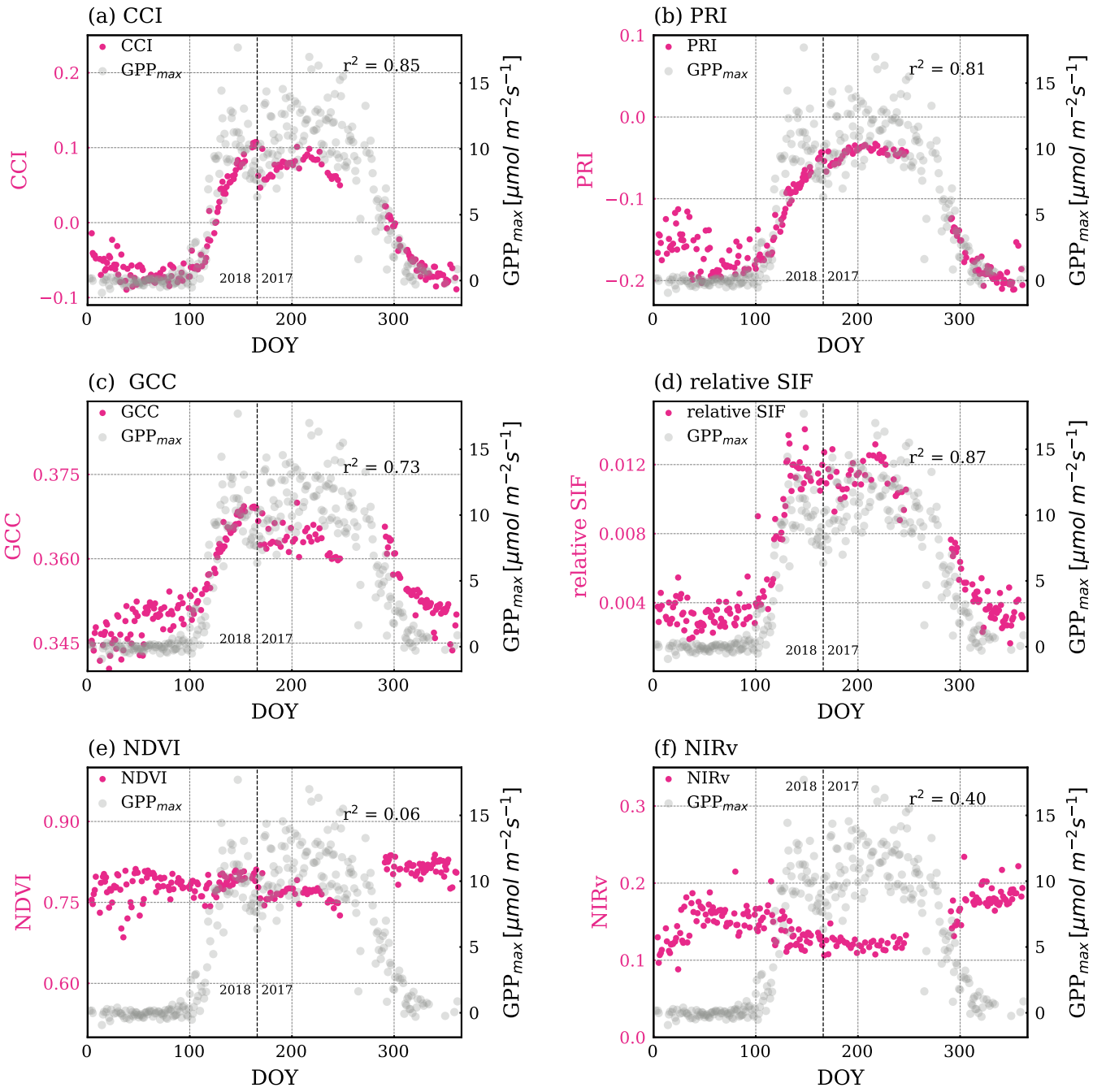

Figure 5. Magenta points are time series of VIs: (a) CCI, (b) PRI, (c) GCC, (d) relative SIF (e) NDVI (f) NIRv.The grey points in the background show GPP_{max}. The Pearson-r^2 values of regressing VIs and GPP_{max} are noted in each plot. The p values of all correlations in this figure are less than 0.005. The vertical dashed line divides the observations from DOY for year 2017 and 2018.

3.3 PLSR coefficients of reflectance with GPP_{max} and pigment measurements

The spectral shape of the PLSR coefficient with GPP_{max} [..[166]]highlighted a peak (centering at [..[167]]532 nm) near that of the carotenoid Jacobian with the same valley-trough feature observed near the second peak of the chlorophyll Jacobian (Fig. 6(a)). [..[168]]

The reconstructed GPP_{max} [..[169]]captured the onset and cessation of growth, while the day-to-day noise in reflectance during dormancy [..[170]]propagated to the reconstructed GPP_{max} [..[171]](-2 to 5 μmol $m^{-2}s^{-1}$). During the growing season, the day-to-day variations in GPP_{max} [..[172]]were not captured by any of the methods using pigment absorption features (Fig. 5(a-c) and Fig. 6(b)), which indicates those [..[173]]variations were not related to pigment content, but rather changes in environmental conditions that lead to [..[174]]day-to-day changes in photosynthesis [..[175]](Fig. S3a). Overall, the observed GPP_{max} [..[176]]was significantly correlated with the PLSR reconstruction (Pearson-r^2=0.87), but very similar compared to CCI and PRI. A similar PLSR model of reflectance but with pigment measurements (Fig. 7) [..[178]]showed a direct link between pigment contents and reflectance. It can be seen that the PLSR coefficients of reflectance are very similar, irrespective of the target variable. They feature a valley near the peak of the carotenoid Jacobian and a valley-trough feature near the peak at the longer wavelength of chlorophyll Jacobian. This spectral shape is also very similar to the second ICA spectral component and PLSR coefficients of GPP_{max}. V+A+Z, chl:car, and car [..[179]]were all nicely reconstructed by using the PLSR coefficients and reflectance (Fig. 7(b)). The reconstructed V+A+Z, car, and chl:car are correlated with the measured ones with Pearson-r^2 values of 0.84, 0.71 and 0.93, respectively.

The second ICA component and PLSR empirically [..[180]]showed the seasonality of reflectance using two different empirical frameworks. ICA only used the reflectance, while the PLSR model accounts for variations in both reflectance and GPP_{max} or pigment content. Yet, both ICA and PLSR agreed on similar spectral features that [..[181]]co-varied seasonally with GPP_{max}. This indicates that the resulting spectral features [..[182]]were primarily responsible for [..[183]]representing this seasonal cycle. The overlap of these features with the chlorophyll/carotenoid absorption features [..[184]]showed that the seasonality of GPP_{max}

[166] removed: highlights
[167] removed: 532.0
[168] removed: All the PLSR coefficients are similar (Fig. S4) because LUEs/GPP_{max} are similar in terms of the seasonal trend.
[169] removed: captures the transition period
[170] removed: propagates
[171] removed: . The high-frequency
[172] removed: during the growing season are
[173] removed: high-frequency variations are
[174] removed: rapid
[175] removed: .
[176] removed: is
[178] removed: shows
[179] removed: are
[180] removed: show
[181] removed: covary seasonally with LUEs/
[182] removed: are
[183] removed: reflecting
[184] removed: shows

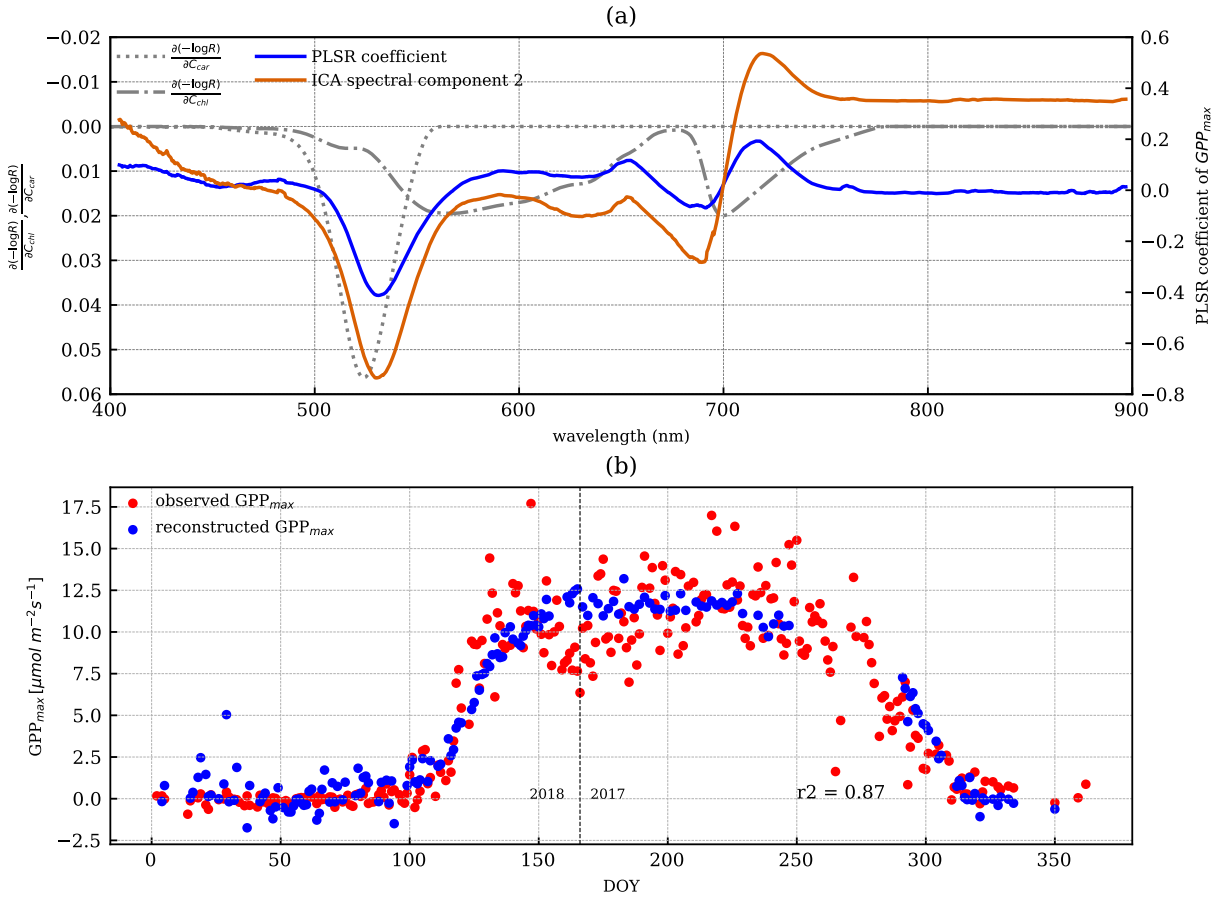

Figure 6. (a) The PLSR [..[177]]coefficient of reflectance with GPP_{max} is the blue line. The overlaid dash-dotted and dotted lines are chlorophyll and carotenoid Jacobians, respectively. The overlaid orange solid line is the second ICA spectral component, which was scaled to fit to the plot without a y-axis. (b) The reconstructed GPP_{max} (blue) by PLSR is overlaid with the observed GPP_{max} (red). The vertical dashed line divides the observations from DOY for year 2017 and 2018.

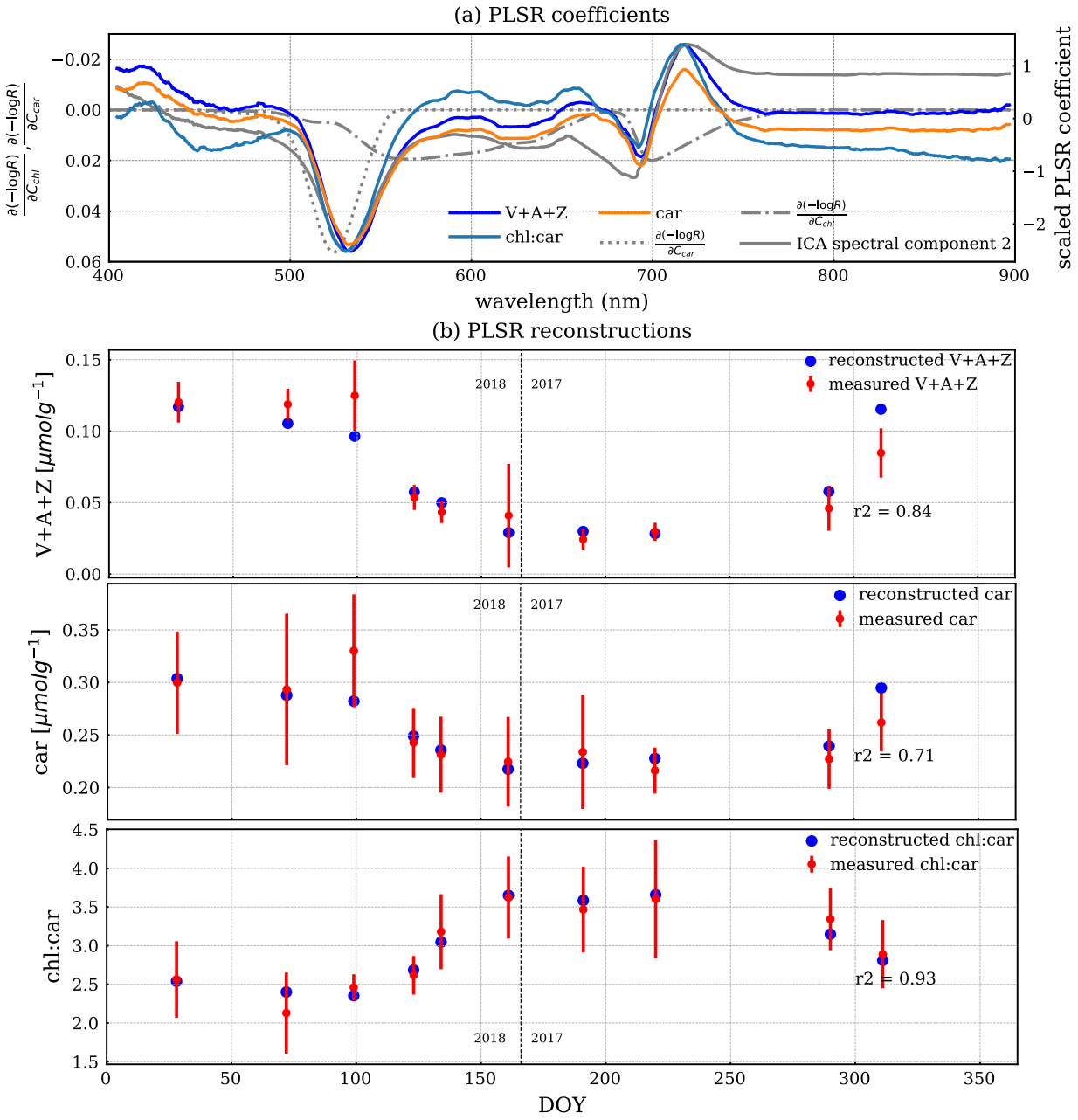

Figure 7. (a) PLSR coefficients of reflectance and three pigment measurements. The overlaid dash-dotted and dotted lines are chlorophyll and carotenoid Jacobians, respectively. The overlaid solid grey line is the second ICA spectral component, which is scaled to fit to the plot without a y-axis. (b) The reconstructed pigment measurements (blue) by PLSR is overlaid with the measured mean pigment measurements (red). The error bar is one standard deviation of the measurements. The vertical dashed line divides the observations from DOY for year 2017 and 2018.

[..[185]]was related to variation in pigment content at the canopy scale, which [..[186]]was directly validated with similar PLSR coefficient of reflectance and pigment contents. These results are consistent with leaf-level measurements of [..[187]]a higher ratio of chlorophyll to carotenoid content during the growing season [..[188]]in this forest (Fig. 7).

The highlighted spectral feature around 530 nm from ICA and PLSR closely overlaps with one of the bands used in CCI, PRI and GCC (Eq. (3)) which provides a justification that these VIs can remarkably capture the LUE seasonality. The comparable Pearson r^2 values of PLSR, CCI, and PRI with GPP_{max} suggest the pigment-driven seasonal cycle of GPP_{max} is sufficiently represented by CCI and PRI. The spectral feature around the red-edge does not make PLSR significantly more correlated with GPP_{max} than CCI or PRI, which implies the feature is not driven by total chlorophyll or carotenoid contents.

3.4 Process-based estimation of pigment content

PROSAIL inversion results further [..[189]]supported the link between canopy reflectance, pigment contents and GPP_{max}. Figure 8 shows a continuous time-series of [..[190]]C_{chl}, [..[191]]C_{car}, Anthocyanin content ([..[192]]C_{ant}), and [..[193]]$\frac{C_{chl}}{C_{car}}$ derived from the PROSAIL canopy RTM inversion model. Examples of simulated and measured reflectance spectra shown are in Fig. C1. Anthocyanins are another type of photoprotective pigment (Pietrini et al., 2002; Lee and Gould, 2002; Gould, 2004) that protects the plants from high light intensity (Hughes, 2011). The pigment inversions closely [..[194]]matched the seasonality of GPP_{max}. [..[195]]$\frac{C_{chl}}{C_{car}}$ showed the greatest sensitivity in capturing the seasonal cycle, with the strongest correlation to leaf level measurements [..[196]](Fig. 8 (c)). The inverted [..[197]]C_{chl} [..[198]]had the weakest empirical relationship with the measured one (Fig. 8(a) right panel). Apparently, some of the inversion errors of individual [..[199]]C_{car} and [..[200]]C_{chl} contents [..[201]]canceled out in the ratio, making the ratio more stable. [..[202]]C_{ant} [..[203]]performed similarly as [..[204]]C_{car}, since they both are photoprotective, and the anthocyanins absorb at 550 nm (Sims and Gamon, 2002), which is close to the center of carotenoid

[185] removed: is
[186] removed: is
[187] removed: chlorophyll contents, which were shown to not change throughout the year; meanwhile,
[188] removed: was detected
[189] removed: supports
[190] removed: Cchl
[191] removed: Ccar
[192] removed: Cant
[193] removed: $\frac{Cchl}{Ccar}$ as
[194] removed: match
[195] removed: $\frac{Cchl}{Ccar}$ shows
[196] removed: . The inversed
[197] removed: Cchl
[198] removed: has
[199] removed: Ccar
[200] removed: Cchl
[201] removed: cancel
[202] removed: Cant
[203] removed: performs similarly as
[204] removed: Ccar

absorption feature. Even though we [..[205]]lacked field measurements of anthocyanins to validate anthocyanins retrievals, the inversions [..[206]]showed that more than just carotenoid content can be obtained from full-spectral inversions.

Strictly speaking, the complex canopy structure of evergreens makes the application of 1D canopy RTMs such as PROSAIL difficult (Jacquemoud et al., 2009; Zarco-Tejada et al., 2019). Yet, Moorthy et al. (2008); Ali et al. (2016); Zarco-Tejada et al. (2019) reasonably discussed the pigment retrieval in conifer forests with careful applications. In our study, the reflectance was collected from needles with a very small FOV, and our study site has a very stable canopy structure throughout a year (Burns et al., 2016). Thus, the inversion results are meaningful for discussing the seasonality of pigment contents. In the future, radiative transfer models that properly describe conifer forests, such as LIBERTY (Dawson et al., 1998), could be used.

3.5 Comparison across methods

Although decomposing the hyperspectral canopy reflectance and using relative SIF (Fig. 5(d)) both successfully [..[213]]tracked the seasonal cycle of evergreen LUE, they underlie different de-excitation processes. During the growing season, environmental conditions primarily [..[214]]drove the day-to-day variations in GPP_{max}. Relative SIF [..[215]]responded to such environmental stresses (van der Tol et al., 2014) so that it [..[216]]appeared to track sub-seasonal variations better than reflectance[..[217]], particularly during the growing season (Fig. S5f). Yet, reflectance decompositions and VIs were less sensitive to such day-to-day variations (Fig.6, Fig. S3b).

There [..[218]]was also some variability between reflectance-based methods and relative SIF during the transition periods between the growing season and dormancy. We [..[219]]focused on the growing season onset since the reflectance measurements [..[220]]were not available during the cessation period. The onset (DOY 60 to 166) described by all the methods mentioned above as well as the relative SIF [..[221]]are compared in Fig. 9, using a sigmoid fit to available data [..[222]](Fig. D1). The observed GPP_{max} [..[223]]had the most rapid yet latest growing onset. The methods and VIs derived from or related to the pigment contents increased earlier than GPP_{max} - such as the ICA component, PLSR coefficient, PROSAIL [..[224]]$\frac{C_{chl}}{C_{car}}$ and CCI. However, they [..[225]]built up slowly to reach the maximum, which suggests that reduction of the carotenoid content is a slower process than the recovery of LUE. Reflectance-based VIs (Fig. 5) and decomposing methods (Fig. 4 and 8(b,c)) [..[226]]had a slower growing

[205] removed: lack
[206] removed: show
[213] removed: track
[214] removed: drive the high-frequency variations in LUEs/
[215] removed: responds
[216] removed: appears to track seasonal and diurnal
[217] removed: .
[218] removed: is
[219] removed: focus
[220] removed: are
[221] removed: from Magney et al. (2019)
[222] removed: .
[223] removed: has
[224] removed: $\frac{Cchl}{Ccar}$
[225] removed: build
[226] removed: have

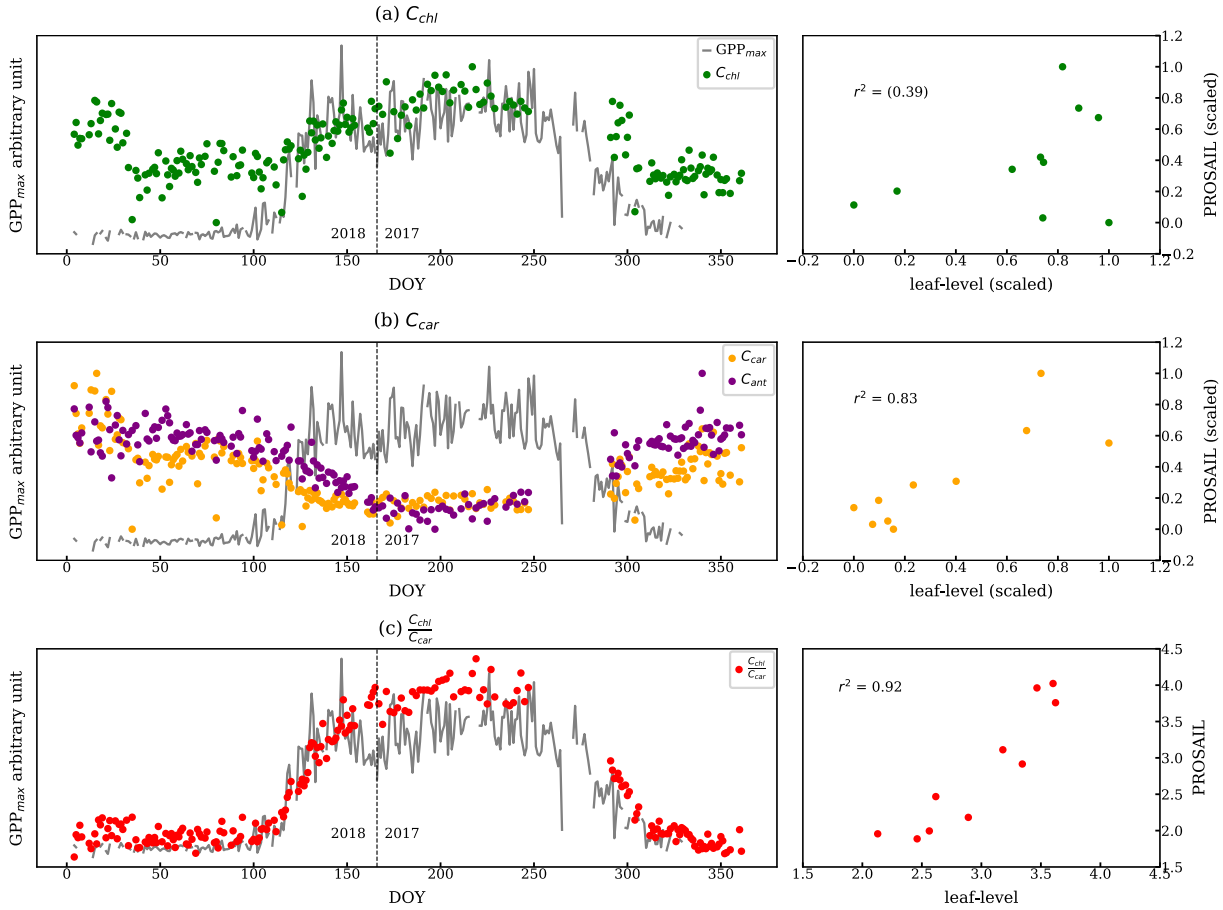

Figure 8. The left panels are the estimations of (a) [..[207]]C_{chl}, (b) [..[208]]C_{car}, [..[209]]C_{ant} and (c) [..[210]]$\frac{C_{chl}}{C_{car}}$ from the PROSAIL overlaid with the GPP$_{\max}$. We normalized two metrics because they report the pigment contents in different units. The vertical dashed line divides the observations from DOY for year 2017 and 2018. The plots on the right compare the pigment contents from leaf-level measurements and using PROSAIL: (a) chl vs. C_{chl}, (b) car vs. C_{car}, and [..[211]](c) chl:car vs. $\frac{C_{chl}}{C_{car}}$. The correlations are statistically significant except [..[212]]C_{chl}.

season onset than GPP_{max}, as found in Bowling et al. (2018) as well. On the other hand, relative SIF started the onset at almost the same time as the GPP_{max}, and it quickly reached the maximum. Therefore, using both SIF and reflectance to constrain the LUE prediction (van der Tol et al., 2014) can further improve the prediction accuracy.

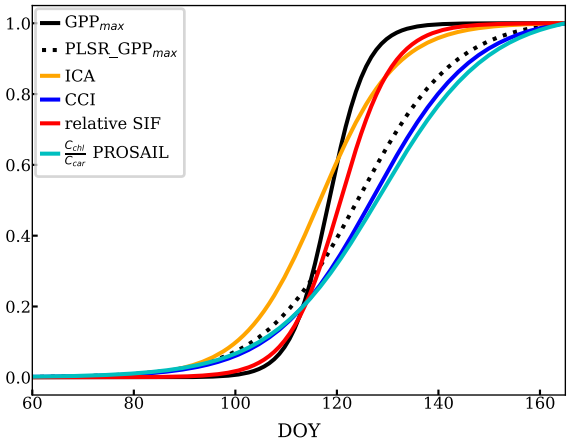

Figure 9. Temporal evolution of [..[227]]the growing season onset using sigmoid fits (scaled) of PLSR, ICA, CCI, chlorophyll to carotenoid ratio and relative SIF.

4 Conclusion and future work

In this study, we analyzed seasonal co-variation of GPP and the spectrally resolved [..[228]]visible and near infrared reflectance signal, as well as several commonly used VIs. The main spectral feature centered around 530 [..[229]]nm is most important for [..[230]]inferring the seasonal cycle of reflectance (400 – 900 nm) and LUE, which corresponds to changes in carotenoid content. This explains why CCI, PRI, and GCC track GPP seasonality so well, as most variations are driven by carotenoid pool changes. Our analysis included RTM simulation and in-situ pigment measurements throughout the season[..[231]], confirming the link between reflectance/VIs and pigment contents. The comparison of reflectance/VIs and relative SIF reveals differences in the timing of the growing season onset, pigment changes and SIF, indicating the potential of using both reflectance and SIF to track the seasonality of photosynthesis. However, the close correspondence between both SIF and reflectance suggest that hyperspectral reflectance alone provides mechanistic evidence for a robust approach to track photosynthetic phenology of evergreen systems. Because seasonal variation in pigment concentration plays a strong role in regulating the seasonality of photosynthesis in evergreen systems, our work will help to inform future studies using hyperspectral reflectance to achieve

[228] removed: VIS-NIR
[229] removed:
[230] removed: explaining
[231] removed: confirms

accurate monitoring of these ecosystems. While indices like PRI and CCI are performing [..[232]]sufficiently as our methods which uses the full spectrum analysis at the canopy scale, the application of the full spectrum might be more robust for space-based measurements. In addition, we [..[233]]found seasonal changes of canopy reflectance [..[234]]near the red-edge region, which could be related to leaf structural changes or chlorophyll-a and b changes. Our PLSR coefficients are good references for customizing VIs to infer the photosynthetic seasonality in evergreen forest when there are restrictions to use the specific bands from currently existing VIs (such as PRI and CCI). While our current study is limited to a subalpine evergreen forest and canopy-scale measurements, applications to other regions, vegetation types and observational platforms will be a focus for future research.

Code and data availability. Our data presented in this paper are provided at https://data.caltech.edu. The PROSAIL model in the Julia programming language used in our study can be obtained from https://github.com/climate-machine/LSM-SPAM.

Appendix A: Bi-directional reflectance effect

A1 NDVI and NIRv

The impact of geometry and small FOV are relatively negligible. First, our method only used the scans when FOV is on the needles by setting a NDVI threshold. Second, we plotted the NDVI and NIRv against the solar geometry at each individual tree targets throughout a year. NDVI/NIRv are quite homogeneous regardless of various solar geometries as shown in the following figures.

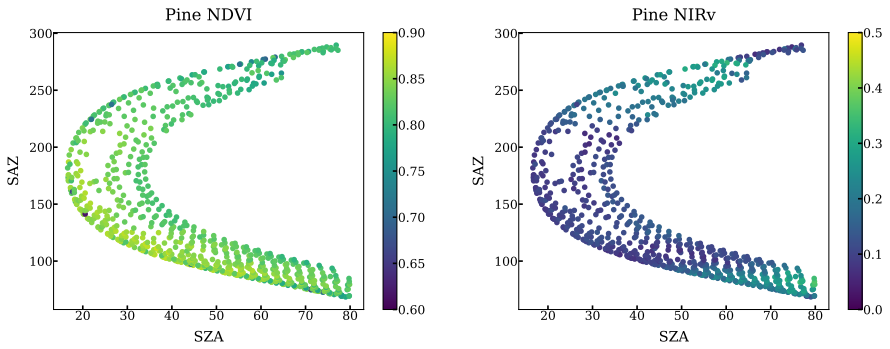

Figure A1. NDVI and NIRv of all scans targeting on a pine at different solar [..[235]]azimuth angles and solar zenith angles throughout a year.

[232]removed: as well as our methods using
[233]removed: find
[234]removed: nearby

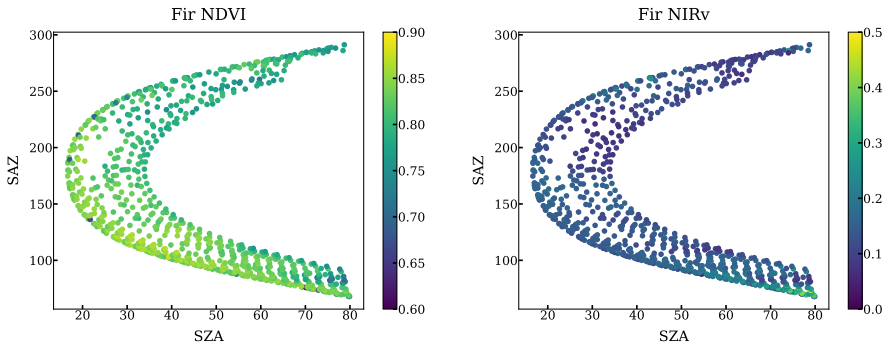

Figure A2. NDVI and NIRv of all scans targeting on a fir at different solar [..[236]]azimuth angles and solar zenith angles throughout a year.

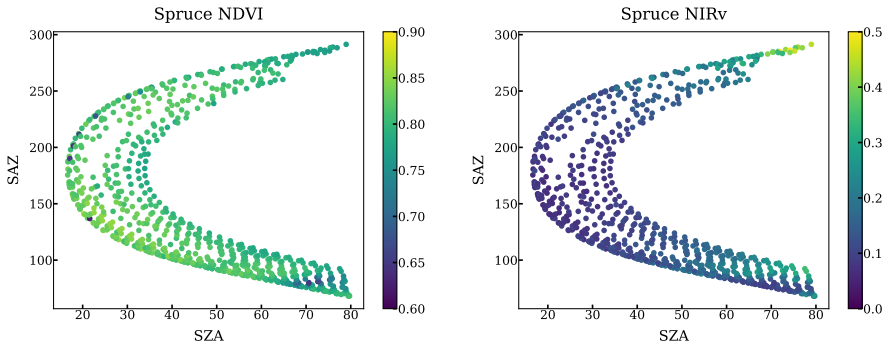

Figure A3. NDVI and NIRv of all scans targeting on a spruce at different solar [..[237]]azimuth angles and solar zenith angles throughout a year.

A2 PLSR on phase angle and reflectance

We did a PLSR analysis on individual measurements of phase angle and reflectance for 3 summer days (2017-7-1 to 2017-7-3). The results are the same from other sample days. Indeed, the reflectance has different sensitivities to the phase angle. However, the poor correlation of PLSR reconstructed phase angle and the measured one suggests the variations in phase angle should not be the critical factor for the change in reflectance. In our study, we primarily removed the bi-directional impact by averaging all the individual reflectance that was measured at different solar geometry and viewing geometry.

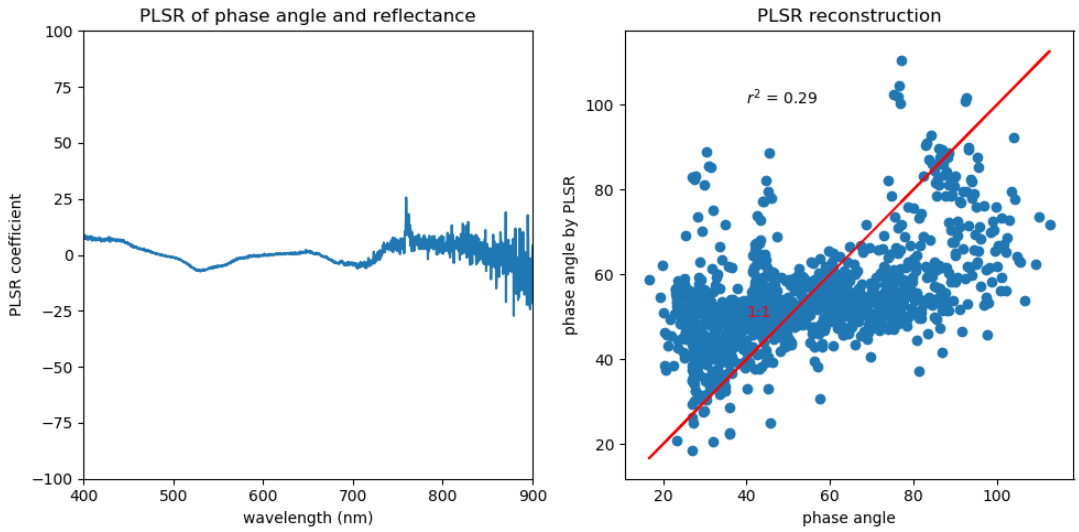

Figure A4. PLSR analysis on phase angle and reflectance.

Appendix B: Detailed processes on integrating daily-averaged canopy reflectance

First, we chose scans targeting vegetation only by requiring an NDVI greater than 0.6. Second, it is important to ensure that the solar irradiation did not change between the acquisition of the solar irradiance and the reflected radiance measurement. To achieve this, we matched the timestamps of a PAR sensor (LI-COR LI-190SA, LI-COR Environmental, Lincoln, Nebraska, US) to the timestamps of PhotoSpec, and compared the PAR value from the PAR sensor during the PhotoSpec irradiance acquisition with PAR during the actual target scan of the reflected radiance from vegetation. We only used the scans when the ratio of the two was 1.0±0.1, ensuring stable PAR conditions. Third, in order to avoid unstable PAR because of clouds (Dye, 2004), we also removed cloudy scenes by requiring PAR to be at least 60% of a theoretical maximum driven by solar geometry (Fig. B1). Further, only data when PAR was greater than 100 μmol $m^{-2}s^{-1}$ were considered to eliminate the impact of low solar angles on reflectance data. The VIs shown in Fig. 5 were extracted in the same fashion as above.

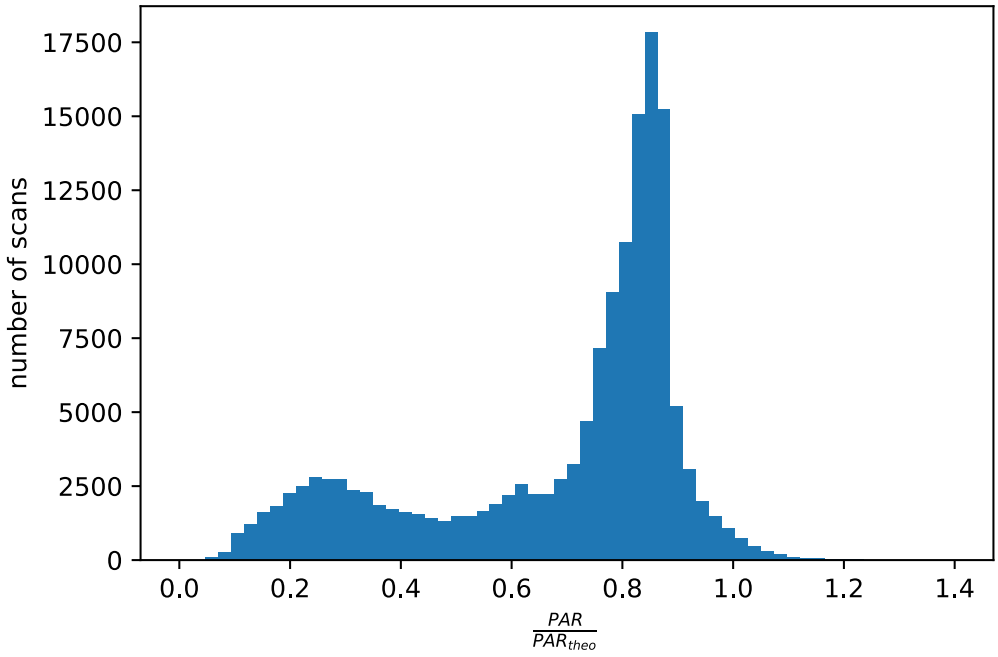

Figure B1. The distribution of ratio the measured PAR to [..[238]]the PAR at theoretical maximum from all individual scans.

Appendix C: PROSAIL fits

We used the following range constraints for variables included in the state vector of PROSAIL inversion:

- Leaf mesophyll structure (N): 0.9–1.1
- Chlorophyll content ([..[239]]C_{chl}): 0–120 μmol cm^{-2}
- Carotenoid content([..[240]]C_{car}): 0–70 μmol cm^{-2}
- Anthocyanin content([..[241]]C_{ant}): 0–10 μmol cm^{-2}
- Brown pigments([..[242]]C_{brown}): 0–0.6
- Water content ([..[243]]C_w): 0–0.2 cm
- Dry matter content ([..[244]]C_m): 0–0.2 g cm^{-2}

[239]removed: Cchl
[240]removed: Car
[241]removed: Ant
[242]removed: Cbrown
[243]removed: Cw
[244]removed: Cm

- [..[245]]Xanthophyll cycle status ([..[246]]C_x) 0–1
- Leaf area index (LAI): fixed to 4.2

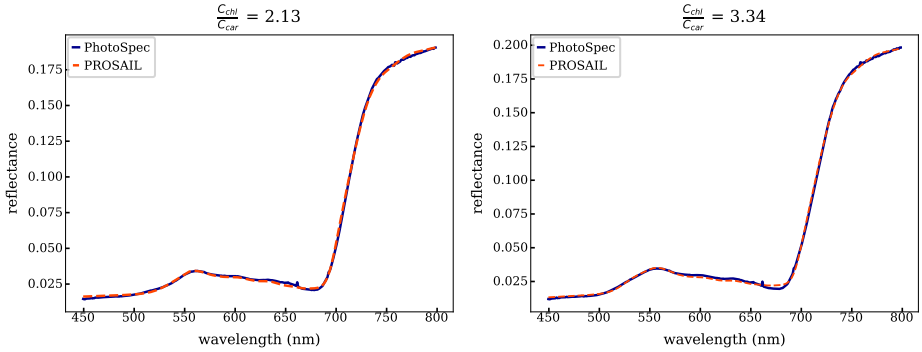

Figure C1. The observed and fitted reflectance spectra at low (left) and high (right) [..[247]]$\frac{C_{chl}}{C_{car}}$

Appendix D: Sigmoid fit

The sigmoid equation is:

$$y = b + \frac{a-b}{1+exp(\frac{d-x}{c})}$$

In this form, a and b represent the maximum and minimum values of the sigmoid fit. And d is the half maximum of the fit. We obtained the optimal values of these parameters.

Proof:

If $x \to +\infty$, $exp(\frac{d-x}{c}) \to 0$. So,

$$\lim_{x \to +\infty} y = a$$

If $x \to -\infty$, $exp(\frac{d-x}{c}) \to +\infty$. So,

$$\lim_{x \to -\infty} y = b$$

The first derivative of y is

$$\frac{dy}{dx} = \frac{a-b}{(1+exp(\frac{d-x}{c}))^2} exp(\frac{d-x}{c}) \frac{1}{c}$$

At the half maximum point (x = x_{half}), $y = \frac{a+b}{2}$. Therefore, we need to solve:

$$\frac{a+b}{2} = b + \frac{a-b}{1+exp(\frac{d-x_{half}}{c})}$$

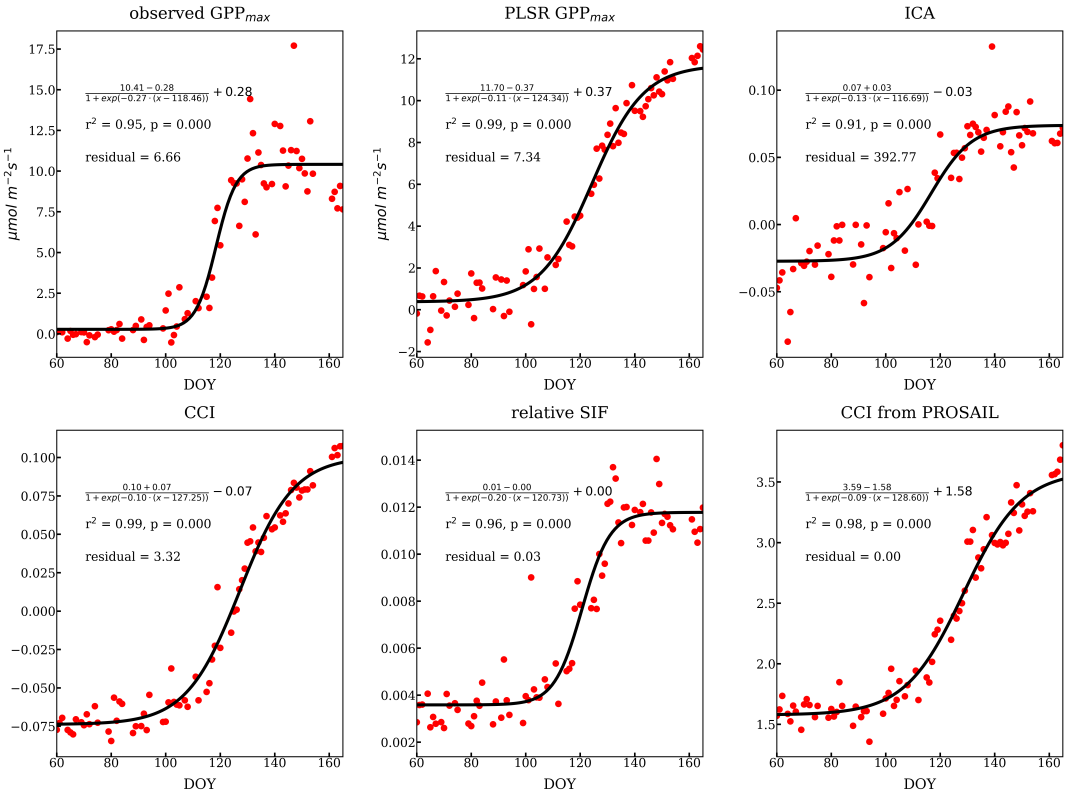

Figure D1. [..[248]]Individual sigmoid fits of the onset of growth from different methods and more VIs. The [..[249]]fitted curve has been expressed as the [..[250]]derivation as above. The pearson-r^2 and p values listed in each subplot were calculated from the [..[251]]correlation of [..[252]]observed and fitted variables. The residual was calculated as the average L2 norm of the difference between observed (y) and fitted variables ($\hat{y}$) normalized by the observation, i.e. $\frac{1}{n}\sum_i(\frac{y-\hat{y}}{y})^2$. The fittings are overall good. Because the ICA loading lacks a clear sigmoid shape, ICA has a larger residual.

Hence, x_{half} = d.

Author contributions. RC, TSM, DD, and CF designed research. RC, TSM, DD, DRB, BAL, SPB, PDB, KG, SL, ADR, JS, and CF performed data analyses. RC, TSM, DD, DRB, BAL, SPB, PDB, KG, SL, ADR, JS, and CF wrote the paper.

Competing interests. I declare that neither I nor my co-authors have any competing interests.

[245]removed: Xantophyll

[246]removed: Cx

Acknowledgements. We thank the sponsors from the Caltech Graduate First-year Fellowship, NASA Carbon Monitoring Systems program (Award NNX16AP33G) to D. R. Bowling. The US-NR1 AmeriFlux site has been supported by the U.S. DOE, Office of Science through the AmeriFlux Management Project (AMP) at Lawrence Berkeley National Laboratory under Award Number 7094866. The National Center for Atmospheric Research (NCAR) is sponsored by NSF.

References

Adams, W. W. and Demmig-Adams, B.: Carotenoid composition and down regulation of photosystem II in three conifer species during the winter, Physiologia Plantarum, 92, 451–458, https://doi.org/10.1111/j.1399-3054.1994.tb08835.x, http://doi.wiley.com/10.1111/j.1399-3054.1994.tb08835.x, 1994.

Ahlström, A., Schurgers, G., Arneth, A., and Smith, B.: Robustness and uncertainty in terrestrial ecosystem carbon response to CMIP5 climate change projections, Environmental Research Letters, 7, 044 008, https://doi.org/10.1088/1748-9326/7/4/044008, http://stacks.iop.org/1748-9326/7/i=4/a=044008?key=crossref.c334ef142bc600447b618d3813e5e3ce, 2012.

Ali, A. M., Darvishzadeh, R., Skidmore, A. K., van Duren, I., Heiden, U., and Heurich, M.: Estimating leaf functional traits by inversion of PROSPECT: Assessing leaf dry matter content and specific leaf area in mixed mountainous forest, International journal of applied earth observation and geoinformation, 45, 66–76, 2016.

Asner, G. P., Martin, R. E., Knapp, D. E., Tupayachi, R., Anderson, C., Carranza, L., Martinez, P., Houcheime, M., Sinca, F., and Weiss, P.: Spectroscopy of canopy chemicals in humid tropical forests, Remote Sensing of Environment, 115, 3587–3598, https://doi.org/10.1016/J.RSE.2011.08.020, https://www.sciencedirect.com/science/article/pii/S0034425711003245?via{%}3Dihub, 2011.

Badgley, G., Field, C. B., and Berry, J. A.: Canopy near-infrared reflectance and terrestrial photosynthesis, Science Advances, 3, e1602 244, https://doi.org/10.1126/sciadv.1602244, http://advances.sciencemag.org/lookup/doi/10.1126/sciadv.1602244, 2017.

Baldocchi, D., Falge, E., Gu, L., Olson, R., Hollinger, D., Running, S., Anthoni, P., Bernhofer, C., Davis, K., Evans, R., et al.: FLUXNET: A new tool to study the temporal and spatial variability of ecosystem-scale carbon dioxide, water vapor, and energy flux densities, Bulletin of the American Meteorological Society, 82, 2415–2434, 2001.

Barnes, M. L., Breshears, D. D., Law, D. J., van Leeuwen, W. J. D., Monson, R. K., Fojtik, A. C., Barron-Gafford, G. A., and Moore, D. J. P.: Beyond greenness: Detecting temporal changes in photosynthetic capacity with hyperspectral reflectance data, PLOS ONE, 12, e0189 539, https://doi.org/10.1371/journal.pone.0189539, https://dx.plos.org/10.1371/journal.pone.0189539, 2017.

Blanken, P. D., Monson, R. K., Burns, S. P., Bowling, D. R., and Turnipseed, A. A.: Data and information for the AmeriFlux US-NR1 Niwot Ridge Subalpine Forest (LTER NWT1) Site, AmeriFlux Management Project, Berkeley, CA: Lawrence Berkeley National Laboratory., https://doi.org/r/10.17190/AMF/1246088, 2019.

Bowling, D. and Logan, B.: Carbon Monitoring System (CMS)Conifer Needle Pigment Composition, Niwot Ridge, Colorado, USA, 2017-2018, p. 0.021358 MB, https://doi.org/10.3334/ORNLDAAC/1723, https://daac.ornl.gov/cgi-bin/dsviewer.pl?ds_id=1723, 2019.

Bowling, D. R., Logan, B. A., Hufkens, K., Aubrecht, D. M., Richardson, A. D., Burns, S. P., Anderegg, W. R., Blanken, P. D., and Eiriksson, D. P.: Limitations to winter and spring photosynthesis of a Rocky Mountain subalpine forest, Agricultural and Forest Meteorology, 252, 241–255, https://doi.org/10.1016/J.AGRFORMET.2018.01.025, https://www.sciencedirect.com/science/article/pii/S016819231830025X?via{%}3Dihub, 2018.

Burns, S. P., Blanken, P. D., Turnipseed, A. A., Hu, J., and Monson, R. K.: The influence of warm-season precipitation on the diel cycle of the surface energy balance and carbon dioxide at a Colorado subalpine forest site, Biogeosciences, 12, 7349–7377, https://doi.org/10.5194/bg-12-7349-2015, www.biogeosciences.net/12/7349/2015/, 2015.

Burns, S. P., Maclean, G. D., Blanken, P. D., Oncley, S. P., Semmer, S. R., and Monson, R. K.: The Niwot Ridge Subalpine Forest US-NR1 AmeriFlux site - Part 1: Data acquisition and site record-keeping, Geoscientific Instrumentation, Methods and Data Systems, 5, 451–471, https://doi.org/10.5194/gi-5-451-2016, https://www.geosci-instrum-method-data-syst.net/5/451/2016/, 2016.

Ciais, P., Sabine, C., Bala, G., Bopp, L., Brovkin, V., Canadell, J., Chhabra, R., DeFries, R., Galloway, J., Heimann, M., Jones, C., Le Quéré, C., Myneni, R., Piao, S., and Thornton, P.: Carbon and Other Biogeochemical Cycles, in: Climate Change 2013: The Physical Science Basis. Contribution of Working Group I to the Fifth Assessment Report of the Intergovernmental Panel on Climate Change, edited by Stock, T., Qin, D., Plattner, G.-K., Tignor, M., Allen, S., Boschung, J., Nauels, A., Xia, Y., Bex, V., and Midgley, P., chap. 6, pp. 465–570, Cambridge University Press, Cambridge, United Kingdom and New York, NY, USA, https://doi.org/10.1017/CBO9781107415324.015, 2013.

Comon, P.: Independent component analysis, a new concept?, Signal processing, 36, 287–314, 1994.

Dawson, T. P., Curran, P. J., and Plummer, S. E.: LIBERTY—Modeling the effects of leaf biochemical concentration on reflectance spectra, Remote sensing of environment, 65, 50–60, 1998.

de Tomás Marín, S., Novák, M., Klančnik, K., and Gaberščik, A.: Spectral signatures of conifer needles mainly depend on their physical traits, Polish Journal of Ecology, 64, 1–14, 2016.

Dechant, B., Cuntz, M., Vohland, M., Schulz, E., and Doktor, D.: Estimation of photosynthesis traits from leaf reflectance spectra: correlation to nitrogen content as the dominant mechanism, Remote sensing of environment, 196, 279–292, 2017.

Dechant, B., Ryu, Y., and Kang, M.: Making full use of hyperspectral data for gross primary productivity estimation with multivariate regression: Mechanistic insights from observations and process-based simulations, Remote Sensing of Environment, 234, 111 435, 2019.

Demmig-Adams, B. and Adams, W. W.: The role of xanthophyll cycle carotenoids in the protection of photosynthesis, Trends in Plant Science, 1, 21–26, https://doi.org/10.1016/S1360-1385(96)80019-7, https://www.sciencedirect.com/science/article/pii/S1360138596800197?via{%}3Dihub, 1996.

DuBois, S., Desai, A. R., Singh, A., Serbin, S. P., Goulden, M. L., Baldocchi, D. D., Ma, S., Oechel, W. C., Wharton, S., Kruger, E. L., et al.: Using imaging spectroscopy to detect variation in terrestrial ecosystem productivity across a water-stressed landscape, Ecological applications, 28, 1313–1324, 2018.

Dutta, D., Schimel, D. S., Sun, Y., van der Tol, C., and Frankenberg, C.: Optimal inverse estimation of ecosystem parameters from observations of carbon and energy fluxes, Biogeosciences, 16, 77–103, https://doi.org/10.5194/bg-16-77-2019, https://www.biogeosciences.net/16/77/2019/, 2019.

Dye, D. G.: Spectral composition and quanta-to-energy ratio of diffuse photosynthetically active radiation under diverse cloud conditions, Journal of Geophysical Research, 109, D10 203, https://doi.org/10.1029/2003JD004251, http://doi.wiley.com/10.1029/2003JD004251, 2004.

Farquhar, G. D., von Caemmerer, S., and Berry, J. A.: A biochemical model of photosynthetic CO2 assimilation in leaves of C3 species, Planta, 149, 78–90, https://doi.org/10.1007/BF00386231, http://www.ncbi.nlm.nih.gov/pubmed/24306196http://link.springer.com/10.1007/BF00386231, 1980.

Feret, J.-B., François, C., Asner, G. P., Gitelson, A. A., Martin, R. E., Bidel, L. P., Ustin, S. L., le Maire, G., and Jacquemoud, S.: PROSPECT-4 and 5: Advances in the leaf optical properties model separating photosynthetic pigments, Remote Sensing of Environment, 112, 3030–3043, https://doi.org/10.1016/J.RSE.2008.02.012, https://www.sciencedirect.com/science/article/pii/S0034425708000813?via{%}3Dihub, 2008.

Féret, J. B., Gitelson, A. A., Noble, S. D., and Jacquemoud, S.: PROSPECT-D: Towards modeling leaf optical properties through a complete lifecycle, Remote Sensing of Environment, 193, 204–215, https://doi.org/10.1016/j.rse.2017.03.004, http://dx.doi.org/10.1016/j.rse.2017.03.004, 2017.

Féret, J.-B., Le Maire, G., Jay, S., Berveiller, D., Bendoula, R., Hmimina, G., Cheraiet, A., Oliveira, J., Ponzoni, F., Solanki, T., et al.: Estimating leaf mass per area and equivalent water thickness based on leaf optical properties: Potential and limitations of physical modeling and machine learning, Remote Sensing of Environment, 231, 110 959, 2019.

Gamon, J., Peñuelas, J., and Field, C.: A narrow-waveband spectral index that tracks diurnal changes in photosynthetic efficiency, Remote Sensing of Environment, 41, 35–44, https://doi.org/10.1016/0034-4257(92)90059-S, https://www.sciencedirect.com/science/article/pii/003442579290059S, 1992.

Gamon, J., Rahman, A., Dungan, J., Schildhauer, M., and Huemmrich, K.: Spectral Network (SpecNet)—What is it and why do we need it?, Remote Sensing of Environment, 103, 227–235, https://doi.org/10.1016/J.RSE.2006.04.003, https://www.sciencedirect.com/science/article/pii/S0034425706001301, 2006.

Gamon, J. A., Serrano, L., and Surfus, J. S.: The photochemical reflectance index: an optical indicator of photosynthetic radiation use efficiency across species, functional types, and nutrient levels, Oecologia, 112, 492–501, https://doi.org/10.1007/s004420050337, http://link.springer.com/10.1007/s004420050337, 1997.

Gamon, J. A., Huemmrich, K. F., Wong, C. Y. S., Ensminger, I., Garrity, S., Hollinger, D. Y., Noormets, A., and Peñuelas, J.: A remotely sensed pigment index reveals photosynthetic phenology in evergreen conifers., Proceedings of the National Academy of Sciences of the United States of America, 113, 13 087–13 092, https://doi.org/10.1073/pnas.1606162113, http://www.ncbi.nlm.nih.gov/pubmed/27803333http://www.pubmedcentral.nih.gov/articlerender.fcgi?artid=PMC5135292, 2016.

Garbulsky, M. F., Peñuelas, J., Gamon, J., Inoue, Y., and Filella, I.: The photochemical reflectance index (PRI) and the remote sensing of leaf, canopy and ecosystem radiation use efficiencies: A review and meta-analysis, Remote sensing of environment, 115, 281–297, 2011.

Geladi, P. and Kowalski, B. R.: Partial least-squares regression: a tutorial, Analytica Chimica Acta, 185, 1–17, https://doi.org/10.1016/0003-2670(86)80028-9, https://www.sciencedirect.com/science/article/pii/0003267086800289?via{%}3Dihub, 1986.

Gentine, P. and Alemohammad, S. H.: Reconstructed Solar-Induced Fluorescence: A Machine Learning Vegetation Product Based on MODIS Surface Reflectance to Reproduce GOME-2 Solar-Induced Fluorescence, Geophysical Research Letters, 45, 3136–3146, https://doi.org/10.1002/2017GL076294, 2018.

Genty, B., Briantais, J.-M., and Baker, N. R.: The relationship between the quantum yield of photosynthetic electron transport and quenching of chlorophyll fluorescence, Biochimica et Biophysica Acta (BBA)-General Subjects, 990, 87–92, 1989.

Glenn, E., Huete, A., Nagler, P., Nelson, S., Glenn, E. P., Huete, A. R., Nagler, P. L., and Nelson, S. G.: Relationship Between Remotely-sensed Vegetation Indices, Canopy Attributes and Plant Physiological Processes: What Vegetation Indices Can and Cannot Tell Us About the Landscape, Sensors, 8, 2136–2160, https://doi.org/10.3390/s8042136, http://www.mdpi.com/1424-8220/8/4/2136, 2008.

Gould, K. S.: Nature's Swiss army knife: the diverse protective roles of anthocyanins in leaves, BioMed Research International, 2004, 314–320, 2004.

Goulden, M. L., Munger, J. W., Fan, S.-M., C., D. B., and Wofsy, C. S.: Measurements of carbon sequestration by long-term eddy covariance: methods and a critical evaluation of accuracy, Global Change Biology, 2, 169–182, https://doi.org/10.1111/j.1365-2486.1996.tb00070.x, http://doi.wiley.com/10.1111/j.1365-2486.1996.tb00070.x, 1996.

Grossmann, K., Frankenberg, C., Magney, T. S., Hurlock, S. C., Seibt, U., and Stutz, J.: PhotoSpec: A new instrument to measure spatially distributed red and far-red Solar-Induced Chlorophyll Fluorescence, Remote Sensing of Environment, 216, 311–327, https://doi.org/10.1016/J.RSE.2018.07.002, https://www.sciencedirect.com/science/article/pii/S0034425718303298?via{%}3Dihub, 2018.

Guanter, L., Zhang, Y., Jung, M., Joiner, J., Voigt, M., Berry, J. A., Frankenberg, C., Huete, A. R., Zarco-Tejada, P., Lee, J.-E., et al.: Global and time-resolved monitoring of crop photosynthesis with chlorophyll fluorescence, Proceedings of the National Academy of Sciences, 111, E1327–E1333, 2014.

Hall, F. G., Hilker, T., Coops, N. C., Lyapustin, A., Huemmrich, K. F., Middleton, E., Margolis, H., Drolet, G., and Black, T. A.: Multi-angle remote sensing of forest light use efficiency by observing PRI variation with canopy shadow fraction, Remote Sensing of Environment, 112, 3201–3211, https://doi.org/10.1016/J.RSE.2008.03.015, https://www.sciencedirect.com/science/article/pii/S0034425708001144, 2008.

Harbinson, J.: Modeling the protection of photosynthesis., Proceedings of the National Academy of Sciences of the United States of America, 109, 15 533–4, https://doi.org/10.1073/pnas.1213195109, http://www.ncbi.nlm.nih.gov/pubmed/22991475http://www.pubmedcentral.nih.gov/articlerender.fcgi?artid=PMC3465449, 2012.

Hilker, T., Coops, N. C., Hall, F. G., Nichol, C. J., Lyapustin, A., Black, T. A., Wulder, M. A., Leuning, R., Barr, A., Hollinger, D. Y., Munger, B., and Tucker, C. J.: Inferring terrestrial photosynthetic light use efficiency of temperate ecosystems from space, Journal of Geophysical Research, 116, G03 014, https://doi.org/10.1029/2011JG001692, http://doi.wiley.com/10.1029/2011JG001692, 2011a.

Hilker, T., Gitelson, A., Coops, N. C., Hall, F. G., and Black, T. A.: Tracking plant physiological properties from multi-angular tower-based remote sensing, Oecologia, 165, 865–876, https://doi.org/10.1007/s00442-010-1901-0, http://link.springer.com/10.1007/s00442-010-1901-0, 2011b.

Horler, D. N. H., Dockray, M., and Barber, J.: The red edge of plant leaf reflectance, International Journal of Remote Sensing, 4, 273–288, https://doi.org/10.1080/01431168308948546, https://www.tandfonline.com/doi/full/10.1080/01431168308948546, 1983.

Huemmrich, K. F., Campbell, P. K. E., Gao, B.-C., Flanagan, L. B., and Goulden, M.: ISS as a Platform for Optical Remote Sensing of Ecosystem Carbon Fluxes: A Case Study Using HICO, IEEE Journal of Selected Topics in Applied Earth Observations and Remote Sensing, 10, 4360–4375, https://doi.org/10.1109/JSTARS.2017.2725825, http://ieeexplore.ieee.org/document/8051041/, 2017.

Huemmrich, K. F., Campbell, P., Landis, D., and Middleton, E.: Developing a common globally applicable method for optical remote sensing of ecosystem light use efficiency, Remote Sensing of Environment, 230, 111 190, 2019.

Huete, A., Liu, H., Batchily, K., and Van Leeuwen, W.: A comparison of vegetation indices over a global set of TM images for EOS-MODIS, Remote sensing of environment, 59, 440–451, 1997.

Hughes, N. M.: Winter leaf reddening in 'evergreen'species, New Phytologist, 190, 573–581, 2011.

Hyvärinen, A. and Oja, E.: Independent component analysis: algorithms and applications, Neural Networks, 13, 411–430, https://doi.org/10.1016/S0893-6080(00)00026-5, https://www.sciencedirect.com/science/article/pii/S0893608000000265, 2000.

Jacquemoud, S. and Baret, F.: PROSPECT: A model of leaf optical properties spectra, Remote sensing of environment, 34, 75–91, 1990.

Jacquemoud, S., Baret, F., Andrieu, B., Danson, F., and Jaggard, K.: Extraction of vegetation biophysical parameters by inversion of the PROSPECT + SAIL models on sugar beet canopy reflectance data. Application to TM and AVIRIS sensors, Remote Sensing of Environment, 52, 163–172, https://doi.org/10.1016/0034-4257(95)00018-V, https://www.sciencedirect.com/science/article/pii/003442579500018V, 1995.

Jacquemoud, S., Verhoef, W., Baret, F., Bacour, C., Zarco-Tejada, P. J., Asner, G. P., François, C., and Ustin, S. L.: PROSPECT+ SAIL models: A review of use for vegetation characterization, Remote sensing of environment, 113, S56–S66, 2009.

Krause, G. H. and Weis, E.: CHLOROPHYLL FLUORESCENCE AND PHOTOSYNTHESIS: The Basics, Tech. rep., www.annualreviews.org, 1991.

Krinner, G., Viovy, N., de Noblet-Ducoudré, N., Ogée, J., Polcher, J., Friedlingstein, P., Ciais, P., Sitch, S., and Prentice, I. C.: A dynamic global vegetation model for studies of the coupled atmosphere-biosphere system, Global Biogeochemical Cycles, 19, https://doi.org/10.1029/2003GB002199, http://doi.wiley.com/10.1029/2003GB002199, 2005.

Lee, D. W. and Gould, K. S.: Why leaves turn red: pigments called anthocyanins probably protect leaves from light damage by direct shielding and by scavenging free radicals, American Scientist, 90, 524–531, 2002.

Leuning, R.: A critical appraisal of a combined stomatal-photosynthesis model for C3 plants, Plant, Cell & Environment, 18, 339–355, 1995.

Liu, H. Q. and Huete, A.: A feedback based modification of the NDVI to minimize canopy background and atmospheric noise, IEEE transactions on geoscience and remote sensing, 33, 457–465, 1995.

Magney, T. S., Bowling, D. R., Logan, B. A., Grossman, K., Stutz, J., Blanken, P., Burns, S. P., Cheng, R., Garcia, M. A., Köhler, P., Lopez, S., Parazoo, N., Raczka, B., Schimel, D., and Frankenberg, C.: Mechanistic evidence for tracking the seasonality of photosynthesis with solar induced fluorescence, Proceedings of the National Academy of Sciences of the United States of America., https://doi.org/10.1073/pnas.1900278116, https://www.pnas.org/lookup/doi/10.1073/pnas.1900278116, 2019.

Matthes, J. H., Knox, S. H., Sturtevant, C., Sonnentag, O., Verfaillie, J., and Baldocchi, D.: Predicting landscape-scale CO 2 flux at a pasture and rice paddy with long-term hyperspectral canopy reflectance measurements, Biogeosciences, 12, 4577–4594, https://doi.org/10.5194/bg-12-4577-2015, www.biogeosciences.net/12/4577/2015/, 2015.

Meacham-Hensold, K., Montes, C. M., Wu, J., Guan, K., Fu, P., Ainsworth, E. A., Pederson, T., Moore, C. E., Brown, K. L., Raines, C., and Bernacchi, C. J.: High-throughput field phenotyping using hyperspectral reflectance and partial least squares regression (PLSR) reveals genetic modifications to photosynthetic capacity, Remote Sensing of Environment, p. 111176, https://doi.org/10.1016/J.RSE.2019.04.029, https://www.sciencedirect.com/science/article/pii/S0034425719301804, 2019.

Middleton, E., Huemmrich, K., Landis, D., Black, T., Barr, A., and McCaughey, J.: Photosynthetic efficiency of northern forest ecosystems using a MODIS-derived Photochemical Reflectance Index (PRI), Remote Sensing of Environment, 187, 345–366, 2016.

Monson, R. K., Turnipseed, A. A., Sparks, J. P., Harley, P. C., Scott-Denton, L. E., Sparks, K., and Huxman, T. E.: Carbon sequestration in a high-elevation, subalpine forest, Global Change Biology, 8, 459–478, https://doi.org/10.1046/j.1365-2486.2002.00480.x, http://doi.wiley.com/10.1046/j.1365-2486.2002.00480.x, 2002.

Monson, R. K., Sparks, J. P., Rosenstiel, T. N., Scott-Denton, L. E., Huxman, T. E., Harley, P. C., Turnipseed, A. A., Burns, S. P., Backlund, B., and Hu, J.: Climatic influences on net ecosystem CO 2 exchange during the transition from wintertime carbon source to springtime carbon sink in a high-elevation, subalpine forest, Oecologia, 146, 130–147, 2005.

Monteith, J. L.: Solar Radiation and Productivity in Tropical Ecosystems, Journal of Applied Ecology, 9, 747–766, https://www.jstor.org/stable/2401901, 1972.

Monteith, J. L. and Moss, C. J.: Climate and the Efficiency of Crop Production in Britain and Discussion, Philosophical Transactions of the Royal Society B Biological Sciences, 281, 277–294, 1977.

Moorthy, I., Miller, J. R., and Noland, T. L.: Estimating chlorophyll concentration in conifer needles with hyperspectral data: An assessment at the needle and canopy level, Remote Sensing of Environment, 112, 2824–2838, 2008.

Pietrini, F., Iannelli, M., and Massacci, A.: Anthocyanin accumulation in the illuminated surface of maize leaves enhances protection from photo-inhibitory risks at low temperature, without further limitation to photosynthesis, Plant, Cell & Environment, 25, 1251–1259, 2002.

Porcar-Castell, A., Tyystjärvi, E., Atherton, J., Van der Tol, C., Flexas, J., Pfündel, E. E., Moreno, J., Frankenberg, C., and Berry, J. A.: Linking chlorophyll a fluorescence to photosynthesis for remote sensing applications: mechanisms and challenges, Journal of experimental botany, 65, 4065–4095, 2014.

Porcar-Castell, A., Mac Arthur, A., Rossini, M., Eklundh, L., Pacheco-Labrador, J., Anderson, K., Balzarolo, M., Martín, M., Jin, H., Tomelleri, E., et al.: EUROSPEC: at the interface between remote-sensing and ecosystem CO flux measurements in Europe, Biogeosciences, 12, 6103–6124, 2015.

Rautiainen, M., Lukeš, P., Homolova, L., Hovi, A., Pisek, J., and Mottus, M.: Spectral properties of coniferous forests: A review of in situ and laboratory measurements, Remote Sensing, 10, 207, 2018.

Reichstein, M., Falge, E., Baldocchi, D., Papale, D., Aubinet, M., Berbigier, P., Bernhofer, C., Buchmann, N., Gilmanov, T., Granier, A., Grunwald, T., Havrankova, K., Ilvesniemi, H., Janous, D., Knohl, A., Laurila, T., Lohila, A., Loustau, D., Matteucci, G., Meyers, T., Miglietta, F., Ourcival, J.-M., Pumpanen, J., Rambal, S., Rotenberg, E., Sanz, M., Tenhunen, J., Seufert, G., Vaccari, F., Vesala, T., Yakir, D., and Valentini, R.: On the separation of net ecosystem exchange into assimilation and ecosystem respiration: review and improved algorithm, Global Change Biology, 11, 1424–1439, https://doi.org/10.1111/j.1365-2486.2005.001002.x, http://doi.wiley.com/10.1111/j.1365-2486.2005.001002.x, 2005.

Richardson, A. D., Braswell, B. H., Hollinger, D. Y., Jenkins, J. P., and Ollinger, S. V.: Near-surface remote sensing of spatial and temporal variation in canopy phenology, Ecological Applications, 19, 1417–1428, 2009.

Richardson, A. D., Hufkens, K., Milliman, T., Aubrecht, D. M., Chen, M., Gray, J. M., Johnston, M. R., Keenan, T. F., Klosterman, S. T., Kosmala, M., Melaas, E. K., Friedl, M. A., and Frolking, S.: Tracking vegetation phenology across diverse North American biomes using PhenoCam imagery, Scientific Data, 5, 180 028, https://doi.org/10.1038/sdata.2018.28, http://www.nature.com/articles/sdata201828, 2018.

Robinson, N. P., Allred, B. W., Smith, W. K., Jones, M. O., Moreno, A., Erickson, T. A., Naugle, D. E., and Running, S. W.: Terrestrial primary production for the conterminous United States derived from Landsat 30 m and MODIS 250 m, Remote Sensing in Ecology and Conservation, 4, 264–280, https://doi.org/10.1002/rse2.74, http://doi.wiley.com/10.1002/rse2.74, 2018.

Rook, D. A.: The influence of growing temperature on photosynthesis and respiration of Pinus radiata seedlings, New Zealand Journal of Botany, 7, 43–55, https://doi.org/10.1080/0028825X.1969.10429101, http://www.tandfonline.com/doi/abs/10.1080/0028825X.1969.10429101, 1969.

Rouse Jr, J., Haas, R., Schell, J., and Deering, D.: Monitoring vegetation systems in the Great Plains with ERTS, Third ERTS Symposium, NASA SP-351.1., pp. 309–317, 1974.

Running, S. W., Nemani, R. R., Heinsch, F. A., Zhao, M., Reeves, M., and Hashimoto, H.: A Continuous Satellite-Derived Measure of Global Terrestrial Primary Production, BioScience, 54, 547–560, https://doi.org/10.1641/0006-3568(2004)054[0547:acsmog]2.0.co;2, https://academic.oup.com/bioscience/article/54/6/547/294347, 2004.

Schreiber, U., Schliwa, U., and Bilger, W.: Continuous recording of photochemical and non-photochemical chlorophyll fluorescence quenching with a new type of modulation fluorometer, Photosynthesis research, 10, 51–62, 1986.

Serbin, S. P., Dillaway, D. N., Kruger, E. L., and Townsend, P. A.: Leaf optical properties reflect variation in photosynthetic metabolism and its sensitivity to temperature, Journal of Experimental Botany, 63, 489–502, https://doi.org/10.1093/jxb/err294, https://academic.oup.com/jxb/article-lookup/doi/10.1093/jxb/err294, 2012.

Serbin, S. P., Singh, A., McNeil, B. E., Kingdon, C. C., and Townsend, P. A.: Spectroscopic determination of leaf morphological and biochemical traits for northern temperate and boreal tree species, Ecological Applications, 24, 1651–1669, 2014.

Serbin, S. P., Singh, A., Desai, A. R., Dubois, S. G., Jablonski, A. D., Kingdon, C. C., Kruger, E. L., and Townsend, P. A.: Remotely estimating photosynthetic capacity, and its response to temperature, in vegetation canopies using imaging spectroscopy, Remote Sensing of Environment, 167, 78–87, 2015.

Silva-Perez, V., Molero, G., Serbin, S. P., Condon, A. G., Reynolds, M. P., Furbank, R. T., and Evans, J. R.: Hyperspectral reflectance as a tool to measure biochemical and physiological traits in wheat, Journal of Experimental Botany, 69, 483–496, https://doi.org/10.1093/jxb/erx421, https://academic.oup.com/jxb/article/69/3/483/4772616, 2018.

Sims, D. A. and Gamon, J. A.: Relationships between leaf pigment content and spectral reflectance across a wide range of species, leaf structures and developmental stages, Remote sensing of environment, 81, 337–354, 2002.

Singh, A., Serbin, S. P., McNeil, B. E., Kingdon, C. C., and Townsend, P. A.: Imaging spectroscopy algorithms for mapping canopy foliar chemical and morphological traits and their uncertainties, Ecological Applications, 25, 2180–2197, 2015.

Smith, M.-L., Ollinger, S. V., Martin, M. E., Aber, J. D., Hallett, R. A., and Goodale, C. L.: Direct estimation of aboveground forest productivity through hyperspectral remote sensing of canopy nitrogen, Ecological applications, 12, 1286–1302, 2002.

Sonnentag, O., Hufkens, K., Teshera-Sterne, C., Young, A. M., Friedl, M., Braswell, B. H., Milliman, T., O'Keefe, J., and Richardson, A. D.: Digital repeat photography for phenological research in forest ecosystems, Agricultural and Forest Meteorology, 152, 159–177, https://doi.org/10.1016/J.AGRFORMET.2011.09.009, https://www.sciencedirect.com/science/article/pii/S0168192311002851, 2012.

Stylinski, C., Gamon, J., and Oechel, W.: Seasonal patterns of reflectance indices, carotenoid pigments and photosynthesis of evergreen chaparral species, Oecologia, 131, 366–374, https://doi.org/10.1007/s00442-002-0905-9, http://link.springer.com/10.1007/s00442-002-0905-9, 2002.

Tucker, C. J.: Red and photographic infrared linear combinations for monitoring vegetation, Remote Sensing of Environment, 8, 127–150, https://doi.org/10.1016/0034-4257(79)90013-0, https://www.sciencedirect.com/science/article/pii/0034425779900130, 1979.

Ustin, S. L., Roberts, D. A., Gamon, J. A., Asner, G. P., and Green, R. O.: Using imaging spectroscopy to study ecosystem processes and properties, BioScience, 54, 523–534, 2004.

Ustin, S. L., Gitelson, A. A., Jacquemoud, S., Schaepman, M., Asner, G. P., Gamon, J. A., and Zarco-Tejada, P.: Retrieval of foliar information about plant pigment systems from high resolution spectroscopy, Remote Sensing of Environment, 113, S67–S77, 2009.

van der Tol, C., Berry, J. A., Campbell, P. K. E., and Rascher, U.: Models of fluorescence and photosynthesis for interpreting measurements of solar-induced chlorophyll fluorescence, Journal of Geophysical Research: Biogeosciences, 119, 2312–2327, https://doi.org/10.1002/2014JG002713, http://doi.wiley.com/10.1002/2014JG002713, 2014.

Verhoeven, A. S., Adams, W. W., and Demmig-Adams, B.: Close relationship between the state of the xanthophyll cycle pigments and photosystem II efficiency during recovery from winter stress, Physiologia Plantarum, 96, 567–576, https://doi.org/10.1111/j.1399-3054.1996.tb00228.x, http://doi.wiley.com/10.1111/j.1399-3054.1996.tb00228.x, 1996.

Vilfan, N., Van der Tol, C., Yang, P., Wyber, R., Malenovský, Z., Robinson, S. A., and Verhoef, W.: Extending Fluspect to simulate xanthophyll driven leaf reflectance dynamics, Remote Sensing of Environment, 211, 345–356, https://doi.org/10.1016/J.RSE.2018.04.012, https://www.sciencedirect.com/science/article/pii/S0034425718301573, 2018.

Wingate, L., Ogée, J., Cremonese, E., Filippa, G., Mizunuma, T., Migliavacca, M., Moisy, C., Wilkinson, M., Moureaux, C., Wohlfahrt, G., Hammerle, A., Hörtnagl, L., Gimeno, C., Porcar-Castell, A., Galvagno, M., Nakaji, T., Morison, J., Kolle, O., Knohl, A., Kutsch, W., Kolari, P., Nikinmaa, E., Levula, J., Heinesch, B., Sprintsin, M., Yakir, D., Manise, T., Guyon, D., Ahrends, H., Plaza-Aguilar, A., Guan, J. H., and Grace, J.: Interpreting canopy development and physiology using a European phenology camera network at flux sites, Biogeosciences, 12, 24, https://doi.org/10.5194/bg-12-5995-2015, www.biogeosciences.net/12/5995/2015/, 2015.

Wold, S., Ruhe, A., Wold, H., and Dunn, III, W.: The collinearity problem in linear regression. The partial least squares (PLS) approach to generalized inverses, SIAM Journal on Scientific and Statistical Computing, 5, 735–743, 1984.

Wong, C. Y. and Gamon, J. A.: The photochemical reflectance index provides an optical indicator of spring photosynthetic activation in evergreen conifers, New Phytologist, 206, 196–208, 2015a.

Wong, C. Y., D'Odorico, P., Bhathena, Y., Arain, M. A., and Ensminger, I.: Carotenoid based vegetation indices for accurate monitoring of the phenology of photosynthesis at the leaf-scale in deciduous and evergreen trees, Remote Sensing of Environment, 233, 111 407, https://doi.org/https://doi.org/10.1016/j.rse.2019.111407, http://www.sciencedirect.com/science/article/pii/S0034425719304262, 2019.

Wong, C. Y., D'Odorico, P., Arain, M. A., and Ensminger, I.: Tracking the phenology of photosynthesis using carotenoid-sensitive and near-infrared reflectance vegetation indices in a temperate evergreen and mixed deciduous forest, New Phytologist, 2020.

Wong, C. Y. S. and Gamon, J. A.: Three causes of variation in the photochemical reflectance index (PRI) in evergreen conifers, New Phytologist, 206, https://doi.org/10.1111/nph.13159, 2015b.

Woodgate, W., Suarez, L., van Gorsel, E., Cernusak, L., Dempsey, R., Devilla, R., Held, A., Hill, M., and Norton, A.: tri-PRI: A three band reflectance index tracking dynamic photoprotective mechanisms in a mature eucalypt forest, Agricultural and Forest Meteorology, 272-273, 187–201, https://doi.org/10.1016/J.AGRFORMET.2019.03.020, https://www.sciencedirect.com/science/article/pii/S0168192319301327?via{%}3Dihub, 2019.

Wutzler, T., Lucas-Moffat, A., Migliavacca, M., Knauer, J., Sickel, K., Šigut, L., Menzer, O., and Reichstein, M.: Basic and extensible post-processing of eddy covariance flux data with REddyProc, Biogeosciences, 15, 5015–5030, https://doi.org/10.5194/bg-15-5015-2018, https://doi.org/10.5194/bg-15-5015-2018, 2018.

Xiao, X., Hollinger, D., Aber, J., Goltz, M., Davidson, E. A., Zhang, Q., and Moore, B.: Satellite-based modeling of gross primary production in an evergreen needleleaf forest, Remote Sensing of Environment, 89, 519–534, https://doi.org/10.1016/j.rse.2003.11.008, 2004.

Yang, P. and van der Tol, C.: Linking canopy scattering of far-red sun-induced chlorophyll fluorescence with reflectance, Remote sensing of environment, 209, 456–467, 2018.

Zarco-Tejada, P., Hornero, A., Beck, P., Kattenborn, T., Kempeneers, P., and Hernández-Clemente, R.: Chlorophyll content estimation in an open-canopy conifer forest with Sentinel-2A and hyperspectral imagery in the context of forest decline, Remote sensing of environment, 223, 320–335, 2019.

Zarter, C. R., Adams, W. W., Ebbert, V., Cuthbertson, D. J., Adamska, I., and Demmig-Adams, B.: Winter down-regulation of intrinsic photosynthetic capacity coupled with up-regulation of Elip-like proteins and persistent energy dissipation in a subalpine forest, New Phytologist, 172, 272–282, https://doi.org/10.1111/j.1469-8137.2006.01815.x, http://doi.wiley.com/10.1111/j.1469-8137.2006.01815.x, 2006.

Zhao, M., Heinsch, F. A., Nemani, R. R., and Running, S. W.: Improvements of the MODIS terrestrial gross and net primary production global data set, Remote Sensing of Environment, 95, 164–176, https://doi.org/10.1016/J.RSE.2004.12.011, https://www.sciencedirect.com/science/article/pii/S0034425705000106, 2005.

Zuromski, L. M., Bowling, D. R., Köhler, P., Frankenberg, C., Goulden, M. L., Blanken, P. D., and Lin, J. C.: Solar-Induced Fluorescence Detects Interannual Variation in Gross Primary Production of Coniferous Forests in the Western United States, Geophysical Research Letters, 45, 7184–7193, https://doi.org/10.1029/2018GL077906, http://doi.wiley.com/10.1029/2018GL077906, 2018.